Theoretical and Applied Fracture Mechanics 128 (2023) 104146

Contents lists available at ScienceDirect

Theoretical and Applied Fracture Mechanics

journal homepage: www.elsevier.com/locate/tafmec

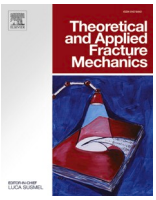

A semi-analytical solution for the in-plane stress fields in isotropic convex finite solids with circular holes reinforced with cylindrically orthotropic rings

Matteo Pastrello, Alessandro Pontefisso, Michele Zappalorto *

University of Padova, Department of Management and Engineering, Stradella San Nicola 3, 36100 Vicenza, Italy

ARTICLE INFO

Keywords:
Reinforced holes
Stress fields
Displacement fields

ABSTRACT

In this paper a semi-analytical solution for the stress distribution in a finite convex plate with a reinforced hole and subjected to a general loading condition is presented. The method described accounts for the geometrical parameters of the plate, as well as material properties and loading conditions, which can be applied internally to the hole boundary and externally to the outside boundaries of the plate. An extensive validation of the proposed solution is carried out comparing the theoretical predictions with results from various finite element analyses, showing an excellent agreement.

1. Introduction

Panels, plates, and shells are among the most common primary elements used in engineering structures, varying widely in shapes but all with the common characteristic of having one geometric dimension much greater or smaller than the other two. The need to meet usual service requirements imposes the necessity to create holes and notches in these elements, hampering the structural strength of such components. Starting from Kirsch in 1898 [1] many authors devoted a great effort to predict the effective stress distributions of plates weakened by such geometrical variations under plane stress or strain hypotheses. Muskhelishvili [2], proposed a complex potential approach for isotropic plates, making easier and more intuitive the study of complex geometries. Lekhnitskii [3] and Savin [4] developed similar approaches for anisotropic materials, using conformal mapping to study holes of various shapes. Many authors later verified and further improved Savin and Muskhelishvili solutions, applying their approaches to holes and notches of different shapes (see [5–12] and reference reported therein). In particular, Batista [5] developed efficient algorithms to calculate stress fields around complex non convex hole shapes, Sharma [13] analyzed polygonal holes, and Rezaeepazhand and Jafari [14] studied metallic panels with special shaped cutouts. Great efforts were also devoted in the recent years to characterize analytically the stress distribution associated to several notch geometries and loading conditions (see [8–12] and references reported therein).

Despite the intense scrutiny carried out on this topic, the subject of notch stress analysis and notch strength still attracts the attention of many researchers (see, among the others, [15–21]).

Within this context, it is worth mentioning that few researchers were able to determine analytical solutions valid on the whole domain of finite bodies weakened by holes or notches with dimensions comparable with the plate size. Within this context, worth mentioning are the pioneering results of Howland [22] and Ling [23] who approached these problems in the first half of the past century, investigating the case of notched strips. More recently, Wah [24] first studied the effect of a circular hole in a polygonal plate, and later Pan et al. [25] analyzed rectangular shaped holes in finite plates. Lin and Ko [26], and Xu et al. [27], instead, developed solutions for a finite composite laminate weakened by an elliptical hole, whereas the problem of finite size bodies under mode III was solved analytically by Salviato and Zappalorto [28,29].

In order to prevent, or reduce, the damage caused by stress concentrations it is possible to reinforce the regions close to holes and notches with stronger and stiffer materials (see for example [30] and references reported therein). Stiff rings, inserts and patches were used, initially, for this purpose. In composites laminates, the strengthening effect can also be obtained by stacking various laminae with grading stiffness (see for example Dave and Sharma [31]). But it is only recently, with additive manufacturing technologies, that functionally graded materials can be effectively engineered (see Yang et al [32]) expanding

* Corresponding author.
E-mail address: michele.zappalorto@unipd.it (M. Zappalorto).

https://doi.org/10.1016/j.tafmec.2023.104146
Received 13 July 2023; Received in revised form 16 October 2023; Accepted 17 October 2023
Available online 19 October 2023
0167-8442/© 2023 The Author(s). Published by Elsevier Ltd. This is an open access article under the CC BY-NC-ND license (http://creativecommons.org/licenses/by-nc-nd/4.0/).

the design flexibility to unprecedented levels. However, the additional degrees of freedom demand new theoretical and numerical tools for driving the design and it is in this perspective that the current research effort finds a valuable place.

The problem of findings analytical solutions for the stress distributions in finite size plates with locally reinforced geometrical variations is that of considerable difficulty, but these solutions would be very useful for engineering applications, especially in the design of additively manufactured mechanical components.

Within this field of research, the main aim of this paper is to expand the previously developed solution for an infinite plate with a concentrically reinforced hole [30] and to propose a method for deriving stress fields in finite convex plates of arbitrary geometry weakened by a concentrically reinforced hole and subjected to arbitrary loads, applied both to the external boundaries of the plate and internally along the hole surface.

The problem is initially analytically stated in its most generic form, using Muskhelishvili complex potential approach and the general solution for a polarly orthotropic annulus. Several boundary conditions are considered. In particular, the boundary conditions for the hole edges are described and applied exactly by solving the corresponding linear system. External boundary conditions are then approximated by minimizing the square residual stresses and obtaining approximated, yet accurate, stress fields for the entire region of the plate. The accuracy of the proposed solution is checked against the results of a large variety of Finite Element analyses varying all the relevant geometrical parameters of the plate.

2. Analytical solution

2.1. Statement of the problem

Consider a generic convex isotropic plate with a circular hole of radius r_0, surrounded by a concentric polarly orthotropic annulus of thickness s (reinforced region) and outer radius r_1, $(s = r_1 - r_0)$ as shown in Fig. 1. Suppose that the solid is subjected to shear and radial stresses along the hole boundary, that can be expressed in the following Fourier series form:

$$\begin{aligned}\bar{\sigma}_{rr}(\theta) &= S_0 + \sum_{n=1}^{N}\left(S_{n,1}\cos(n\theta) + S_{n,2}\sin(n\theta)\right)\\ \bar{\sigma}_{r\theta}(\theta) &= T_0 + \sum_{n=1}^{N}\left(T_{n,1}\cos(n\theta) + T_{n,2}\sin(n\theta)\right)\end{aligned} \tag{1}$$

where $S_0, T_0, S_{ij}, T_{ij} \in \mathbb{R}\forall i : 1 \le i \le N \in \mathbb{N}; j \in \{1,2\}$. Suppose also that external stresses are applied to the solid's external boundaries, described according to the following Fourier series (see Fig. 1):

$$\sigma^{e}_{ij}(\theta) = \Omega^{ij}_0 + \sum_{n=1}^{M}\left(\Omega^{ij}_{n,1}\cos(n\theta) + \Omega^{ij}_{n,1}\sin(n\theta)\right) \tag{2}$$

where $\Omega^{ij}_0, \Omega^{ij}_{n,p} \in \mathbb{R}\forall n : 1 \le n \le M \in \mathbb{N};\ p \in \{1,2\}$, i and j are the direction perpendicular or tangent to the external surface of the solid in every point.

2.2. Universal form for the stress and displacement fields in the reinforced region (reinforcing annulus)

The reinforced region is an annulus concentric with the hole, made of polarly orthotropic material having principal directions of elasticity in the radial and circumferential directions (Fig. 1). Stress and displacements fields in this region can be sought in the same form used by Pastrello et al. [30]:

$$\begin{aligned}u_r^{(1)} =& A_0\left(\frac{r_0}{r}\right)^{\alpha_0} + a_0\left(\frac{r}{r_1}\right)^{\alpha_0} - E_1\left(\frac{1+d^{-2}}{1+\epsilon^{-2}}\right)\cos\theta + (E_1\cos\theta + F_1\sin\theta)\log\left(\frac{r}{r_0}\right) +\\ &+\sum_{n=1}^{P}\left((A_n\cos n\theta + B_n\sin n\theta)\left(\frac{r_0}{r}\right)^{\alpha_n} + (a_n\cos n\theta + b_n\sin n\theta)\left(\frac{r}{r_1}\right)^{\alpha_n}\right) +\\ &+\sum_{n=2}^{P}\left((E_n\cos n\theta + F_n\sin n\theta)\left(\frac{r_0}{r}\right)^{\beta_n} + (e_n\cos n\theta + f_n\sin n\theta)\left(\frac{r}{r_1}\right)^{\beta_n}\right)\end{aligned} \tag{3}$$

$$\begin{aligned}u_\theta^{(1)} =& F_1\left(\frac{1+d^{-2}}{1+\epsilon^{-2}}\right)\cos\theta - H_0\left(\frac{r_0}{r}\right) + (F_1\cos\theta - E_1\sin\theta)\log\left(\frac{r}{r_0}\right) +\\ &+\sum_{n=1}^{P}\left((C_n\sin n\theta - D_n\cos n\theta)\left(\frac{r_0}{r}\right)^{\alpha_n} + (c_n\sin n\theta - d_n\cos n\theta)\left(\frac{r}{r_1}\right)^{\alpha_n}\right) +\\ &+\sum_{n=2}^{P}\left((G_n\sin n\theta - H_n\cos n\theta)\left(\frac{r_0}{r}\right)^{\beta_n} + (g_n\sin n\theta - h_n\cos n\theta)\left(\frac{r}{r_1}\right)^{\beta_n}\right)\end{aligned} \tag{4}$$

$$\begin{aligned}\sigma_{rr}^{(1)} =& \frac{G^{(1)}_{\theta r}}{rc^2d_1^2}\left\{\left(\frac{r_0}{r}\right)^{\alpha_0}A_0\left(c^2 - d^2\alpha_0\right) + \left(\frac{r}{r_1}\right)^{\alpha_0}a_0\left(c^2 + d^2\alpha_0\right) +\right.\\ &+E_1\frac{d^4 - \left(c^2\left(1+d^2\right) - d^4\right)\epsilon^2}{d^2\left(1+\epsilon^2\right)}\cos\theta + F_1\frac{d^4 - \left(c^2\left(1+d^2\right) - d^4\right)\epsilon^2}{d^2\left(1+\epsilon^2\right)}\sin\theta +\\ &+\sum_{n=1}^{P}\left[\left(\frac{r_0}{r}\right)^{\alpha_n}\left[\left(A_n\cos(n\theta) + B_n\sin(n\theta)\right)\left(c^2 - d^2\alpha_n\right) + \left(C_n\cos(n\theta) + D_n\sin(n\theta)\right)nc^2\right] +\right.\\ &\left.+\left(\frac{r}{r_1}\right)^{\alpha_n}\left[\left(a_n\cos(n\theta) + b_n\sin(n\theta)\right)\left(c^2 + d^2\alpha_n\right) + \left(c_n\cos(n\theta) + d_n\sin(n\theta)\right)nc^2\right]\right] +\\ &+\sum_{n=2}^{P}\left[\left(\frac{r_0}{r}\right)^{\beta_n}\left[\left(E_n\cos(n\theta) + F_n\sin(n\theta)\right)\left(c^2 - d^2\beta_n\right) + \left(G_n\cos(n\theta) + H_n\sin(n\theta)\right)nc^2\right] +\right.\\ &\left.\left.+\left(\frac{r}{r_1}\right)^{\beta_n}\left[\left(e_n\cos(n\theta) + f_n\sin(n\theta)\right)\left(c^2 + d^2\beta_n\right) + \left(g_n\cos(n\theta) + h_n\sin(n\theta)\right)nc^2\right]\right]\right\}\end{aligned} \tag{5}$$

$$
\begin{aligned}
\sigma_{\theta\theta}^{(1)} &= \frac{G_{\theta r}^{(1)}}{r d^2 \epsilon_1^2}\left\{\left(\frac{r_0}{r}\right)^{\alpha_0} A_0\left(d^2-\epsilon^2\alpha_0\right)+\left(\frac{r}{r_1}\right)^{\alpha_0} a_0\left(d^2+\epsilon^2\alpha_0\right)+\right.\\
&+E_1\frac{\epsilon^2\left(\epsilon^2-d^2\right)}{1+\epsilon^2}\cos\theta+F_1\frac{\epsilon^2\left(\epsilon^2-d^2\right)}{1+\epsilon^2}\sin\theta+\\
&+\sum_{n=1}^{P}\left[\left(\frac{r_0}{r}\right)^{\alpha_n}\left[\left(A_n\cos(n\theta)+B_n\sin(n\theta)\right)\left(d^2-\epsilon^2\alpha_n\right)+\left(C_n\cos(n\theta)+D_n\sin(n\theta)\right)nd^2\right]+\right.\\
&+\left.\left(\frac{r}{r_1}\right)^{\alpha_n}\left[\left(a_n\cos(n\theta)+b_n\sin(n\theta)\right)\left(d^2+\epsilon^2\alpha_n\right)+\left(c_n\cos(n\theta)+d_n\sin(n\theta)\right)nd^2\right]\right]+\\
&+\sum_{n=2}^{P}\left[\left(\frac{r_0}{r}\right)^{\beta_n}\left[\left(E_n\cos(n\theta)+F_n\sin(n\theta)\right)\left(d^2-\epsilon^2\beta_n\right)+\left(G_n\cos(n\theta)+H_n\sin(n\theta)\right)nd^2\right]+\right.\\
&+\left.\left.\left(\frac{r}{r_1}\right)^{\beta_n}\left[\left(e_n\cos(n\theta)+f_n\sin(n\theta)\right)\left(d^2+\epsilon^2\beta_n\right)+\left(g_n\cos(n\theta)+h_n\sin(n\theta)\right)nd^2\right]\right]\right\}
\end{aligned}
\tag{6}
$$

$$
\begin{aligned}
\sigma_{r\theta}^{(1)} &= \frac{G_{\theta r}^{(1)}}{r}\left\{\frac{2r_0H_0}{r}+F_1\frac{d^2-\int^2}{d^2\left(1+\int^2\right)}\cos\theta+E_1\frac{d^2-\int^2}{d^2\left(1+\int^2\right)}\sin\theta+\right.\\
&+\sum_{n=1}^{P}\left[\left(\frac{r_0}{r}\right)^{\alpha_n}\left[n\left(B_n\cos(n\theta)-A_n\sin(n\theta)\right)+\left(D_n\cos(n\theta)-C_n\sin(n\theta)\right)\left(\alpha_n+1\right)\right]+\right.\\
&+\left.\left(\frac{r}{r_1}\right)^{\alpha_n}\left[n\left(b_n\cos(n\theta)-a_n\sin(n\theta)\right)+\left(c_n\sin(n\theta)-d_n\cos(n\theta)\right)\left(\alpha_n-1\right)\right]\right]+\\
&+\sum_{n=2}^{P}\left[\left(\frac{r_0}{r}\right)^{\beta_n}\left[n\left(F_n\cos(n\theta)-E_n\sin(n\theta)\right)+\left(H_n\cos(n\theta)-G_n\sin(n\theta)\right)\left(\beta_n+1\right)\right]+\right.\\
&+\left.\left.\left(\frac{r}{r_1}\right)^{\beta_n}\left[n\left(f_n\cos(n\theta)-e_n\sin(n\theta)\right)+\left(g_n\sin(n\theta)-h_n\cos(n\theta)\right)\left(\beta_n-1\right)\right]\right]\right\}
\end{aligned}
\tag{7}
$$

In Eqs. (3)–(7), the superscript (1) refers to the elastic constants, stresses and displacements of the material the reinforcing region is made of.

Unknowns A_n, a_n, B_n, b_n, C_n, c_n, D_n, d_n, E_n, e_n, F_n, f_n, G_n, g_n, H_n, h_n, $\forall n \le P \in \mathbb{N} \,|\, N, M \le P$ as well as all the other constants in Eqs. (3)–(7) have the same expressions given in Ref. [30].

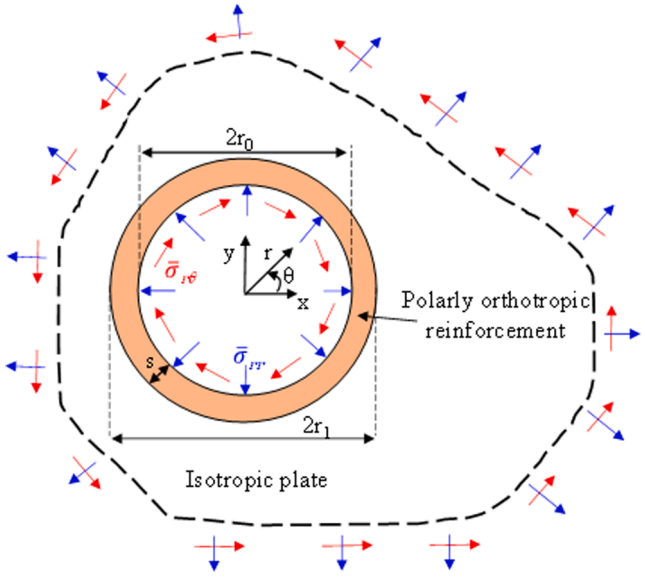

Fig. 1. Finite plate with a reinforced circular hole under generic loading conditions.

2.3. *Universal form for the stress and displacement fields outside the reinforced region (plate)*

The universal form for the stress and displacement fields in the isotropic solid outside the reinforced region can be determined by means of Muskhelishvili formulation [2]:

$$
\begin{aligned}
&\sigma_{rr}^{(2)}+\sigma_{\theta\theta}^{(2)} = 4\mathrm{Re}\left[\frac{d\Phi(z)}{dz}\right]\\
&\sigma_{\theta\theta}^{(2)}-\sigma_{rr}^{(2)}+2i\sigma_{r\theta}^{(2)} = 2e^{2i\theta}\left(\bar{z}\frac{d^2\Phi(z)}{dz^2}+\frac{d\mathrm{X}(z)}{dz}\right)\\
&u_r^{(2)}+iu_\theta^{(2)} = \frac{1+\nu^{(2)}}{E^{(2)}}\left(\kappa\Phi\left(z\right)-z\frac{d\bar{\Phi}(z)}{dz}-\bar{\mathrm{X}(z)}\right)e^{-i\theta}
\end{aligned}
\tag{8}
$$

where E and ν represent the elastic modulus and the Poisson ratio, and superscript (2) identifies the properties of the isotropic unreinforced region.

The following two potential functions are used for the problem under investigation, being them suitable forms to apply proper boundary conditions:

$$
\begin{aligned}
&\Phi(z) = (\bar{A}_0+i\bar{B}_0)log(z)+(\bar{A}_c+i\bar{B}_c)+\sum_{n=1}^{P-1}(\bar{A}_{-n}+i\bar{B}_{-n})z^{-n}+\sum_{n=1}^{P+1}(\bar{A}_n+i\bar{B}_n)z^n\\
&\mathrm{X}(z) = -\kappa(\bar{A}_0-i\bar{B}_0)log(z)+\sum_{n=1}^{P+1}(\bar{C}_{-n}+i\bar{D}_{-n})z^{-n}+\sum_{n=1}^{P-1}(\bar{C}_n+i\bar{D}_n)z^n
\end{aligned}
\tag{9}
$$

Substituting Eq. (9) into Eq. (8) it results in the following stress and displacement fields:

$$
\begin{aligned}
u_r^{(2)} &= \frac{\left(\nu^{(2)}+1\right)}{E^{(2)}}\left\{\frac{\left(r^2(\kappa-1)\bar{A}_1-\bar{C}_{-1}\right)}{r}+\right.\\
&+\frac{\left(r^2\left(\left(\kappa\log\left(r^2\right)-1\right)\bar{A}_0+r^2(\kappa-2)\bar{A}_2+\kappa\bar{A}_c\right)-\bar{C}_{-2}\right)}{r^2}\cos(\theta)+\\
&+\frac{\left(r^2\left(\left(\kappa\log\left(r^2\right)-1\right)\bar{B}_0-r^2(\kappa-2)\bar{B}_2+\kappa\bar{B}_c\right)-\bar{D}_{-2}\right)}{r^2}\sin(\theta)+\\
&+\sum_{n=3}^{P}\left[\frac{\left(r^2((n-1)+\kappa)\bar{A}_{-(n-1)}+r^{2(n+1)}(\kappa-(n+1))\bar{A}_{(n+1)}-\bar{C}_{-(n+1)}-r^{2(n-1)}\bar{C}_{(n-1)}\right)}{r^{n+1}}\cos(n\theta)+\right.\\
&\left.\left.+\frac{\left(r^2((n-1)+\kappa)\bar{B}_{-(n-1)}-r^{2(n+1)}(\kappa-(n+1))\bar{B}_{(n+1)}-\bar{D}_{-(n+1)}+r^{2(n-1)}\bar{D}_{(n-1)}\right)}{r^{n+1}}\sin(n\theta)\right]\right\}
\end{aligned}
\tag{10}
$$

$$
\begin{aligned}
u_\theta^{(2)} &= \frac{\left(\nu^{(2)}+1\right)}{E^{(2)}}\left\{\frac{\left(r^2(1+\kappa)\bar{B}_1+\bar{D}_{-1}\right)}{r}+\right.\\
&+\frac{\left(r^2\left(\left(1+\kappa\log\left(r^2\right)\right)\bar{B}_0+r^2(2+\kappa)\bar{B}_2+\kappa\bar{B}_c\right)+\bar{D}_{-2}\right)}{r^2}\cos(\theta)-\\
&-\frac{\left(r^2\left(\left(1+\kappa\log\left(r^2\right)\right)\bar{A}_0-r^2(2+\kappa)\bar{A}_2+\kappa\bar{A}_c\right)+\bar{C}_{-2}\right)}{r^2}\sin(\theta)+\\
&+\sum_{n=2}^{P}\left[\frac{\left(r^2(\kappa-(n-1))\bar{B}_{-(n-1)}+r^{2(n+1)}(\kappa+(n+1))\bar{B}_{(n+1)}+\bar{D}_{-(n+1)}+r^{2n}\bar{D}_{(n-1)}\right)}{r^{n+1}}\cos(n\theta)-\right.\\
&\left.\left.+\frac{\left(r^2((n-1)-\kappa)\bar{A}_{-(n-1)}+r^{2(n+1)}(\kappa+(n+1))\bar{A}_{(n+1)}-\bar{C}_{-(n+1)}+r^{2n}\bar{C}_{(n-1)}\right)}{r^{n+1}}\sin(n\theta)\right]\right\}
\end{aligned}
\tag{11}
$$

$$
\begin{aligned}
\sigma_{rr}^{(2)} &= \frac{1}{(\widetilde{\nu}-1)}\left\{\frac{\left(\bar{C}_{-1}(\widetilde{\nu}-1)-r^2(\kappa-1)(\widetilde{\nu}+1)\bar{A}_1\right)}{r^2}+\right.\\
&+\frac{2\left(r^2(\widetilde{\nu}-\kappa)\bar{A}_0-r^4(\kappa+\kappa\widetilde{\nu}-2)\bar{A}_2+(\widetilde{\nu}-1)\bar{C}_{-2}\right)}{r^3}\cos(\theta)+\\
&+\frac{2\left(r^2(\widetilde{\nu}-\kappa)\bar{B}_0+r^4(\kappa+\kappa\widetilde{\nu}-2)\bar{B}_2+(\widetilde{\nu}-1)\bar{D}_{-2}\right)}{r^3}\sin(\theta)+\\
&+\sum_{n=2}^{P}\left[\frac{\left((n-1)r^2((n-1)-(n+1)\widetilde{\nu}+\kappa(\widetilde{\nu}+1))\bar{A}_{-(n-1)}+(n+1)(\widetilde{\nu}-1)\bar{C}_{-(n+1)}\right)}{r^{n+1}}\cos(n\theta)-\right.\\
&-\frac{(n+1)r^{2(n+1)}(\kappa-(n+1)+((n-1)+\kappa)\widetilde{\nu})\bar{A}_{(n+1)}+(n-1)(\widetilde{\nu}-1)r^{2n}\bar{C}_{(n-1)}}{r^{n+1}}\cos(n\theta)+\\
&+\frac{\left((n-1)r^2((n-1)-(n+1)\widetilde{\nu}+\kappa(\widetilde{\nu}+1))\bar{B}_{-(n-1)}+(n+1)(\widetilde{\nu}-1)\bar{D}_{-(n+1)}\right)}{r^{n+1}}\sin(n\theta)+\\
&\left.\left.+\frac{(n+1)r^{2(n+1)}(\kappa-(n+1)+((n-1)+\kappa)\widetilde{\nu})\bar{B}_{(n+1)}+(n-1)(\widetilde{\nu}-1)r^{2n}\bar{D}_{(n-1)}}{r^{n+1}}\sin(n\theta)\right]\right\}
\end{aligned}
\tag{12}
$$

$$
\begin{aligned}
\sigma^{(2)}_{\theta\theta} &= \frac{1}{(\widetilde{\nu}-1)}\left\{\frac{(\bar{C}_{-1}(\widetilde{\nu}-1)+r^2(\kappa-1)(\widetilde{\nu}+1)\bar{A}_1)}{r^2}+\right.\\
&+\frac{2(r^2(1-\widetilde{\nu}\kappa)\bar{A}_0+r^4(\kappa+(\kappa-2)\widetilde{\nu})\bar{A}_2-(\widetilde{\nu}-1)\bar{C}_{-2})}{r^3}\cos(\theta)\\
&+\frac{2(r^2(1-\widetilde{\nu}\kappa)\bar{B}_0+r^4(\kappa+(\kappa-2)\widetilde{\nu})\bar{B}_2-(\widetilde{\nu}-1)\bar{D}_{-2})}{r^3}\sin(\theta)+\\
&+\sum_{n=2}^{P}\left[\frac{((n-1)r^2((n-1)\widetilde{\nu}-(n+1)+\kappa(\widetilde{\nu}+1))\bar{A}_{-(n-1)}-(n+1)(\widetilde{\nu}-1)\bar{C}_{-(n+1)})}{r^{n+1}}\cos(n\theta)-\right.\\
&-\frac{(n+1)r^{2(n+1)}((n-1)+\kappa+(\kappa-(n+1))\widetilde{\nu})\bar{A}_{(n+1)}+(n-1)(\widetilde{\nu}-1)r^{2n}\bar{C}_{(n-1)}}{r^{n+1}}\cos(n\theta)+\\
&+\frac{((n-1)r^2((n-1)\widetilde{\nu}-(n+1)+\kappa(\widetilde{\nu}+1))\bar{B}_{-(n-1)}-(n+1)(\widetilde{\nu}-1)\bar{D}_{-(n+1)})}{r^{n+1}}\sin(n\theta)+\\
&\left.\left.+\frac{(n+1)r^{2(n+1)}((n-1)+\kappa+(\kappa-(n+1))\widetilde{\nu})\bar{B}_{(n+1)}+(n-1)(\widetilde{\nu}-1)r^{2n}\bar{D}_{(n-1)}}{r^{n+1}}\sin(n\theta)\right]\right\}
\end{aligned}
\tag{13}
$$

$$
\begin{aligned}
\sigma^{(2)}_{r\theta} &= -\frac{\bar{D}_{-1}}{r^2}+\frac{(r^2(1-\kappa)\bar{B}_0+2(r^4\bar{B}_2+\bar{D}_{-2}))}{r^3}\cos(\theta)+\\
&+\frac{(r^2(1-\kappa)\bar{A}_0+2(r^4\bar{A}_2+\bar{C}_{-2}))}{r^3}\sin(\theta)+\\
&+\sum_{n=2}^{P}\left[\frac{((n^2-n)\bar{B}_{-(n-1)}+(n-1)r^{2n}\bar{D}_{(n-1)}-(n+1)\bar{D}_{-(n+1)}+(n^2+n)r^n\bar{B}_{(n+1)})}{r^{n+2}}\cos(n\theta)+\right.\\
&\left.+\frac{((n+1)\bar{C}_{-(n+1)}+(n-1)r^{2n}\bar{C}_{(n-1)}-(n^2-n)\bar{A}_{-(n-1)}+(n^2+n)r^n\bar{A}_{(n+1)})}{r^{n+2}}\sin(n\theta)\right]\Bigg\}
\end{aligned}
\tag{14}
$$

$\bar{A}_c$, $\bar{B}_c$, $\bar{A}_n$, $\bar{B}_n$, $\bar{C}_n$, $\bar{D}_n$ $\forall n \le P \in \mathbb{N}$ are integration constants to determine applying proper boundary conditions, remembering that $\kappa = 3-4\nu^{(2)}$ for plane strain conditions, whilst for plane stress $\kappa = \frac{3-\nu^{(2)}}{1+\nu^{(2)}}$. $\widetilde{\nu} = \nu^{(2)}$ for plane stress, while $\widetilde{\nu} = \frac{\nu^{(2)}}{1-\nu^{(2)}}$ for plain strain.

2.4. Boundary conditions and explicit solution for unknown coefficients

Since compatibility and equilibrium conditions should be guaranteed along the boundary of the reinforcing annulus, it is possible to write the following system of equations:

$$
\begin{aligned}
&\sigma^{(1)}_{rr}(r=r_0,\theta)=\bar{\sigma}_{rr}(\theta) && \sigma^{(1)}_{r\theta}(r=r_1,\theta)=\sigma^{(2)}_{r\theta}(r=r_1,\theta)\\
&\sigma^{(1)}_{r\theta}(r=r_0,\theta)=\bar{\sigma}_{r\theta}(\theta) && u^{(1)}_{r}(r=r_1,\theta)=u^{(2)}_{r}(r=r_1,\theta)\\
&\sigma^{(1)}_{rr}(r=r_1,\theta)=\sigma^{(2)}_{rr}(r=r_1,\theta) && u^{(1)}_{\theta}(r=r_1,\theta)=u^{(2)}_{\theta}(r=r_1,\theta)
\end{aligned}
\tag{15}
$$

where, $r_1 = r_0 + s$.Eq. (15) can be rewritten in matrix form as it follows:

$$\widehat{\mathbf{H}}\cdot\bar{v}=\bar{k} \tag{16}$$

where $\widehat{\mathbf{H}}$ is a diagonal block matrix defined as:

$$\widehat{\mathbf{H}} = Diag[\widehat{\mathbf{H}}_0, \widehat{\mathbf{H}}_1, \cdots, \widehat{\mathbf{H}}_N] \tag{17}$$

And $\widehat{\mathbf{H}}_i$ are defined in Appendix A. $\bar{v}$ is the coefficient vector:

$$\bar{v} = \{\bar{v}_0, \bar{v}_1, \cdots, \bar{v}_N\} \tag{18}$$

Where:

$$\bar{v}_0 = \{A_0, a_0, \bar{C}_{-1}, \bar{D}_{-1}, H_0, \bar{B}_1\} \tag{19}$$

$$\bar{v}_1 = \{C_1, c_1, E_1, \bar{A}_0, \bar{C}_{-2}, \bar{A}_c, D_1, d_1, F_1, \bar{B}_0, \bar{D}_{-2}, \bar{B}_c\} \tag{20}$$

$$\bar{v}_n = \{C_n, G_n, c_n, g_n, \bar{A}_{1-n}, \bar{C}_{-n-1}, D_n, H_n, d_n, h_n, \bar{B}_{1-n}, \bar{D}_{-n-1}\} \forall\, 2 \le n \le P \tag{21}$$

and $\bar{k}$ is a vector defined in Appendix A.

Solving the system given by Eq. (16) yields expressions for coefficients $\bar{v}$ as functions of the remaining coefficients: $\bar{A}_1$, $\bar{A}_2$, $\bar{B}_2$, $\bar{A}_{n+1}$, $\bar{B}_{n+1}$, $\bar{C}_{n-1}$, $\bar{D}_{n-1}$ with n ranging from 2 to P.

In order to calculate these coefficients, boundary conditions have to be imposed on the external boundaries. Traditional equilibrium equations however cannot be solved exactly for a finite value of P, so a numerical approximation relying on the minimization of the residual stresses is used in this work. The external boundary can be divided into N_{div} number of divisions, each described with parametric equations $l_n(s)$, $n \in \{1, \cdots, N_{div}\}$ (for $N_{div} = 1$, $l_1(s)$ is the parametric description of the whole external boundary).

The residual stresses calculated along these curves are:

$$\Delta^n_{ij} = \left\{\sigma^{(2)}_{ij}(r,\theta) - \sigma^{g}_{ij}(\theta)\right\}\Big|_{\{r,\theta\}\in l_n(s)} \tag{22}$$

where $\sigma^g_{ij}(r)$ are the stresses applied to the external boundary with i, j being the directions perpendicular or tangent to the boundary.

Considering the maximum distance of the external boundaries from the centre of the hole, r_{max}, with the aim to normalize the minimization procedure to the maximum size of the solid it is possible to apply the following substitutions in (22):

$$\bar{A}_n = \frac{\widehat{A}_n}{r^n_{\max}};\ \bar{B}_n = \frac{\widehat{B}_n}{r^n_{\max}};\ \bar{C}_n = \frac{\widehat{C}_n}{r^n_{\max}};\ \bar{D}_n = \frac{\widehat{D}_n}{r^n_{\max}} \tag{23}$$

with n ranging from 2 to P. From (22) and (23) the following function describing the total residual stresses can be defined:

Table 1
Coordinate list of the points used in the convergence analysis.

Point	r coordinate	θ coordinate	Material phase
P1	r_0	0	CFRP
P2	r_1	0	CFRP
P3	r_1	0	GFRP

$$FO = \sum_{n=1}^{N_{div}} \left\{ \int_{l_n} \left[\sum_{i,j} \left(\Delta_{ij}^{n} \right)^2 \right] ds \right\} \tag{24}$$

Function FO is a convex function in the variables $\widehat{A}_1, \widehat{A}_2, \widehat{B}_2, \widehat{A}_{n+1}, \widehat{B}_{n+1}, \widehat{C}_{n-1}, \widehat{D}_{n-1}$ with n ranging from 2 to P, and has only one minimum to be found by solving the linear system:

$$\nabla FO = \underline{0} \tag{25}$$

Eventually, solving (25) and substituting the results into the solutions of system (16) yields an expression for all the coefficients of Eqs. (3)–(7), and (10)–(14).

3. Particular case: the isotropic reinforced annulus

Let us consider the case of an isotropic annulus of internal radius r_0, external radius r_2 and reinforced by a polarly orthotropic material of width $s = r_1 - r_0$. The following internal pressures are applied:

$$\begin{aligned} \bar{\sigma}_{rr}(\theta) &= S_0 + \sum_{n=2}^{N} \left(S_{n,1}\cos(n\theta) + S_{n,2}\sin(n\theta) \right) \\ \bar{\sigma}_{r\theta}(\theta) &= T_0 + \sum_{n=2}^{N} \left(T_{n,1}\cos(n\theta) + T_{n,2}\sin(n\theta) \right) \end{aligned} \tag{26}$$

where $S_0,\ S_{ij},\ T_{ij} \in \mathbb{R} \forall i : 2 \le i \le N \in \mathbb{N}; j \in \{1,2\}$. Moreover, the following stresses are applied at the outer boundary of the annulus:

$$\begin{aligned} \sigma_{rr}^{g}(\theta) &= \Omega_0 + \sum_{n=2}^{M} \left(\Omega_{n,1}\cos(n\theta) + \Omega_{n,2}\sin(n\theta) \right) \\ \sigma_{r\theta}^{g}(\theta) &= \left(\frac{r_0}{r_2} \right)^2 T_0 + \sum_{n=2}^{M} \left(\Psi_{n,1}\cos(n\theta) + \Psi_{n,2}\sin(n\theta) \right) \end{aligned} \tag{27}$$

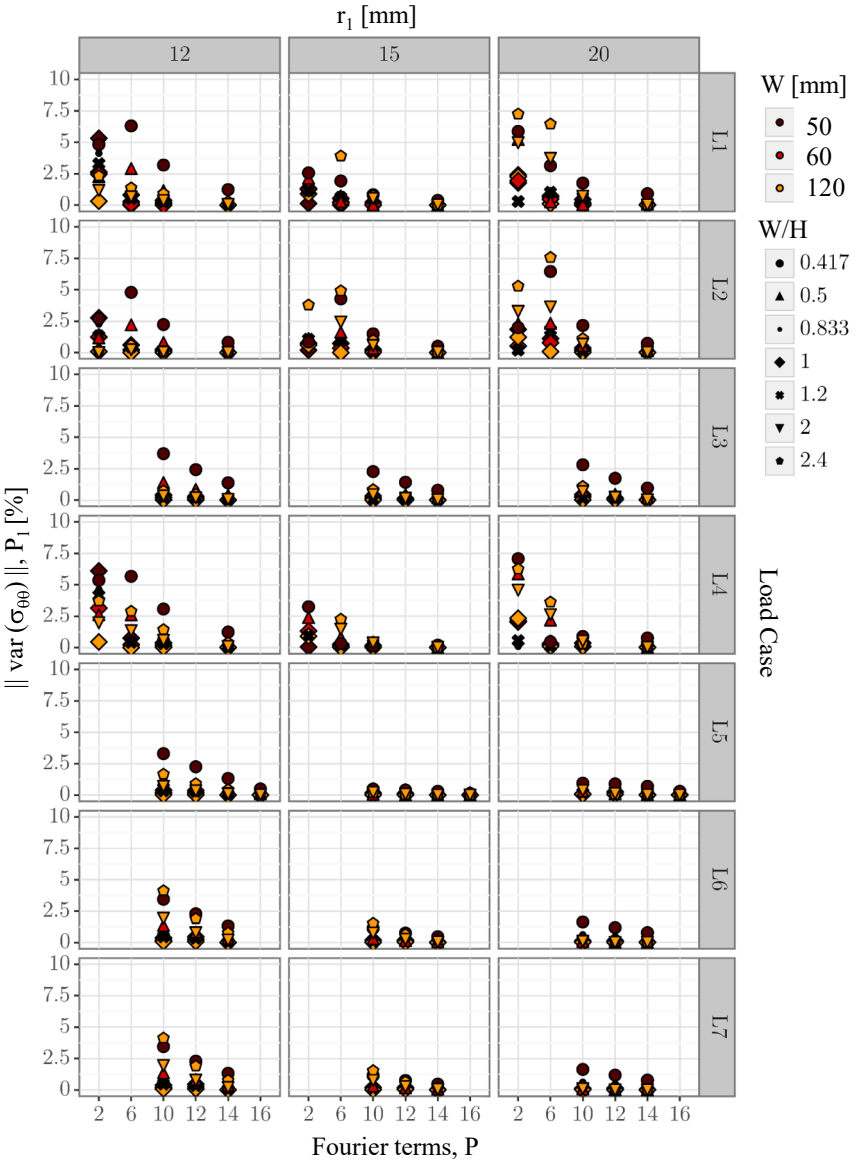

Fig. 2. Convergence analysis for $\sigma_{\theta\theta}$ at point P1 for rectangular plates of width W and height H, under different load cases and r_1 values.

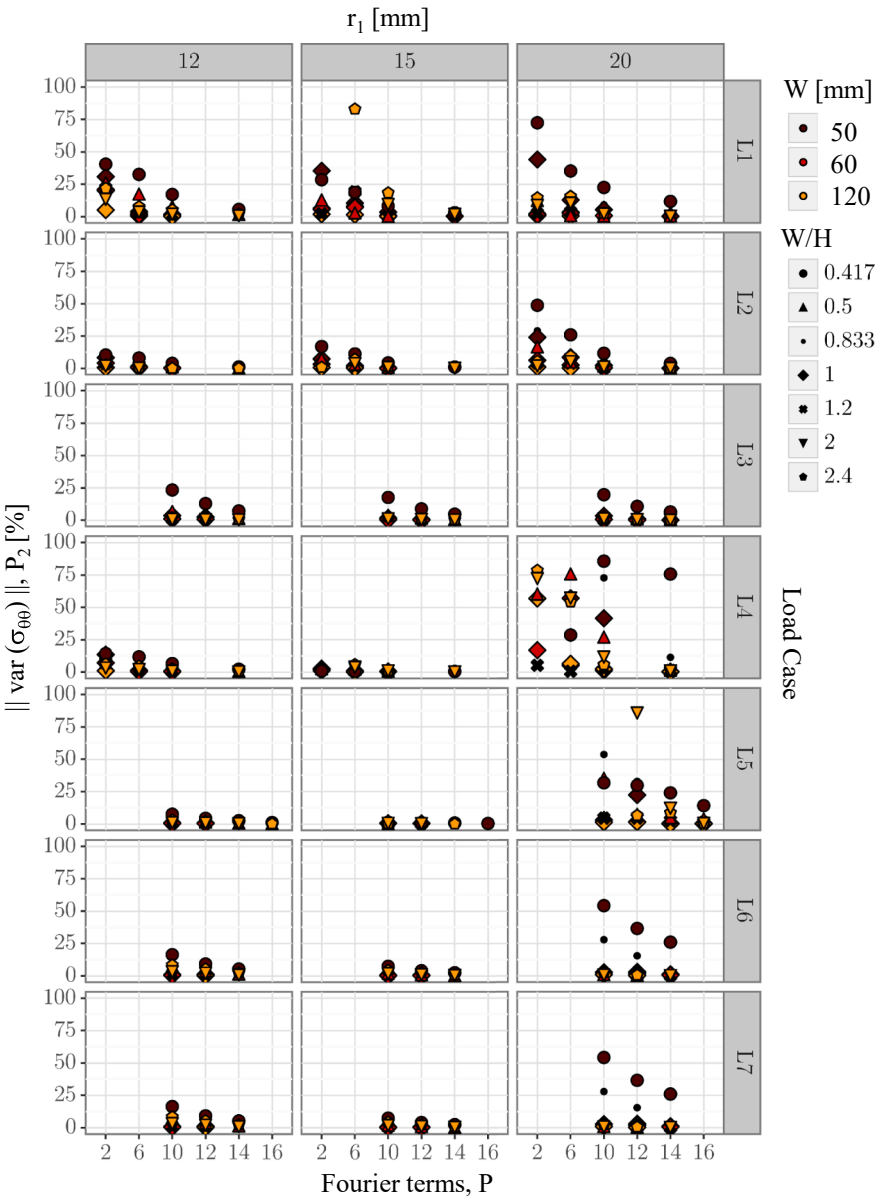

Fig. 3. Convergence analysis for $\sigma_{\theta\theta}$ at point P2 for rectangular plates of width W and height H, under different load cases and r_1 values.

$\Omega_0, \Omega_{ij}, \Psi_{ij} \in \mathbb{R} \forall i : 2 \leq i \leq M \in \mathbb{N}; j \in \{1,2\}$

This particular problem can be solved exactly imposing the boundary conditions:

$$\begin{aligned}
&\sigma_{rr}^{(1)}(r=r_0,\theta) = \bar{\sigma}_{rr}(\theta) && \sigma_{rr}^{(2)}(r=r_2,\theta) = \sigma_{rr}^{g}(\theta)\\
&\sigma_{r\theta}^{(1)}(r=r_0,\theta) = \bar{\sigma}_{r\theta}(\theta) && \sigma_{r\theta}^{(2)}(r=r_2,\theta) = \sigma_{r\theta}^{g}(\theta)\\
&\sigma_{rr}^{(1)}(r=r_1,\theta) = \sigma_{rr}^{(2)}(r=r_1,\theta) && u_{\theta}^{(1)}(r=r_1,\theta) = u_{\theta}^{(2)}(r=r_1,\theta)\\
&\sigma_{r\theta}^{(1)}(r=r_1,\theta) = \sigma_{r\theta}^{(2)}(r=r_1,\theta) && u_{r}^{(1)}(r=r_1,\theta) = u_{r}^{(2)}(r=r_1,\theta)
\end{aligned} \tag{28}$$

Eq. (14) can be rewritten in matrix form as follows:

$$\widehat{\mathbf{H}}^{*} \cdot \bar{\mathrm{v}}^{*} = \bar{\mathrm{k}}^{*} \tag{29}$$

where $\widehat{\mathbf{H}}^{*}$ is a diagonal block matrix defined as:

$$\widehat{\mathbf{H}}^{*} = \mathrm{Diag}\left[\widehat{\mathbf{H}}_0^{*}, \widehat{\mathbf{H}}_1^{*}, \cdots, \widehat{\mathbf{H}}_N^{*}\right] \tag{30}$$

And $\widehat{\mathbf{H}}_i^{*}$ are defined in Appendix B. $\bar{\mathrm{v}}^{*}$ is the coefficient vector:

$$\bar{\mathrm{v}}^{*} = \left\{\bar{\mathrm{v}}_0^{*}, \bar{\mathrm{v}}_1^{*}, \cdots, \bar{\mathrm{v}}_N^{*}\right\} \tag{31}$$

where:

$$\bar{\mathrm{v}}_0^{*} = \{A_0, a_0, \bar{C}_{-1}, \bar{A}_1, \bar{D}_{-1}, H_0, \bar{B}_1\} \tag{32}$$

$$\bar{\mathrm{v}}_1^{*} = \{C_1, c_1, E_1, \bar{A}_0, \bar{C}_{-2}, \bar{A}_c, \bar{A}_2, D_1, d_1, F_1, \bar{B}_0, \bar{D}_{-2}, \bar{B}_c, \bar{B}_2\} \tag{33}$$

and

$$\bar{\mathrm{v}}_n^{*} = \{C_n, G_n, c_n, g_n, \bar{A}_{1-n}, \bar{C}_{-n-1}, \bar{A}_{n+1}, \bar{C}_{n-1}, D_n, H_n, d_n, h_n, \bar{B}_{1-n}, \bar{D}_{-n-1}, \bar{B}_{n+1}, \bar{D}_{n-1}\} \forall 2 \leq n \leq P \tag{34}$$

and $\bar{\mathrm{k}}^{*}$ is a vector defined in Appendix B.

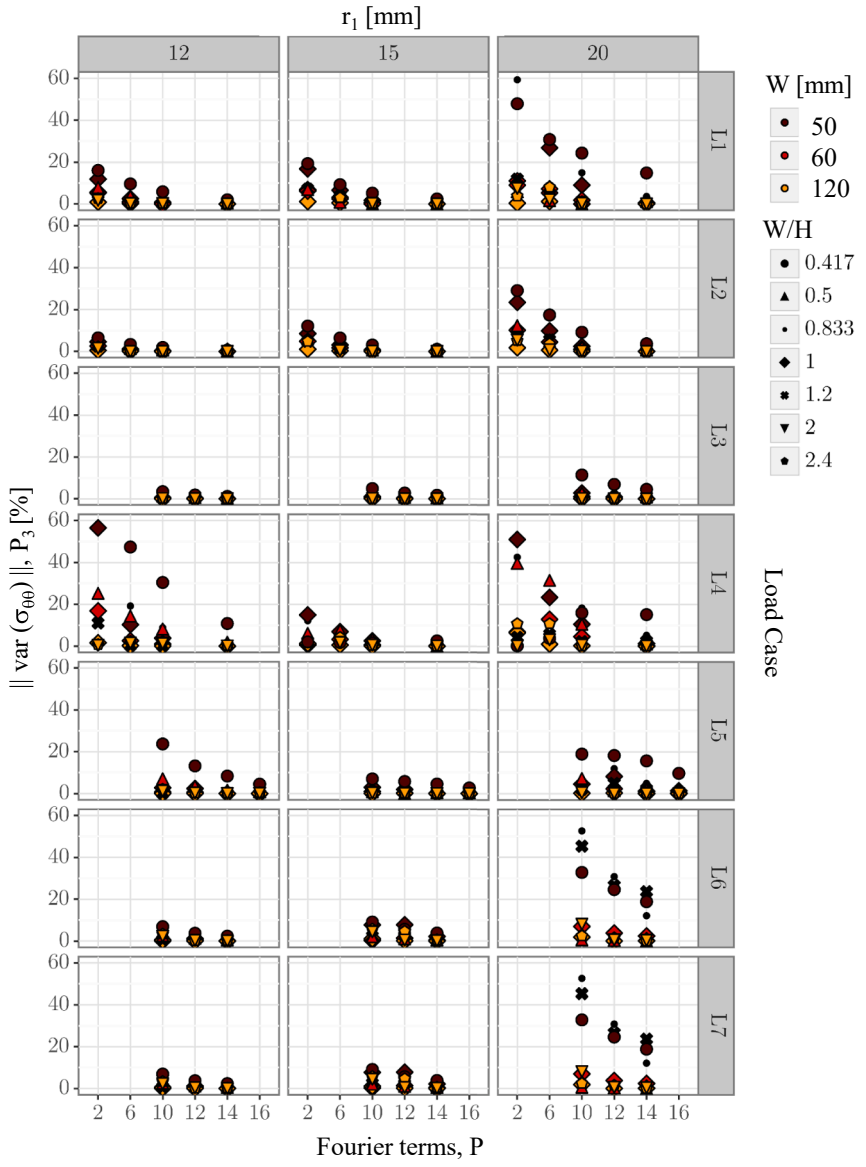

Fig. 4. Convergence analysis for $\sigma_{\theta\theta}$ at point P3 for rectangular plates of width W and height H, under different load cases and r_1 values.

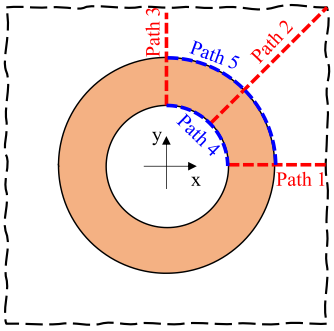

Fig. 5. Schematics of the paths used for comparing the analytical solution with numerical (FE) results.

4. Discussion and comparison with numerical results

4.1. Convergence analysis

Since the proposed solution relies on a numerical approximation, a convergence analysis is due. To this end, different boundary conditions have been applied to a set of rectangular plates with different width W, height H, internal radius r_0 and interface radius r_1, while increasing the number of Fourier terms, P, used for approximating the loads.

The following load cases have been considered:

1. **L1**: uniaxial tension, with $\sigma^g_{yy} = 100\,MPa$.
2. **L2**: biaxial tension, with $\sigma^g_{yy} = 100\,MPa$ and $\sigma^g_{xx} = 50MPa$, and internal pressure $\bar{\sigma}_{rr} = 100\,MPa$.
3. **L3**: biaxial tension, with $\sigma^g_{yy} = 100\,MPa$ and $\sigma^g_{xx} = 50MPa$, and non-uniform internal pressure. In this case, an internal pressure approximating a stress distribution enacted by a pin was described taking advantage of the following equation:

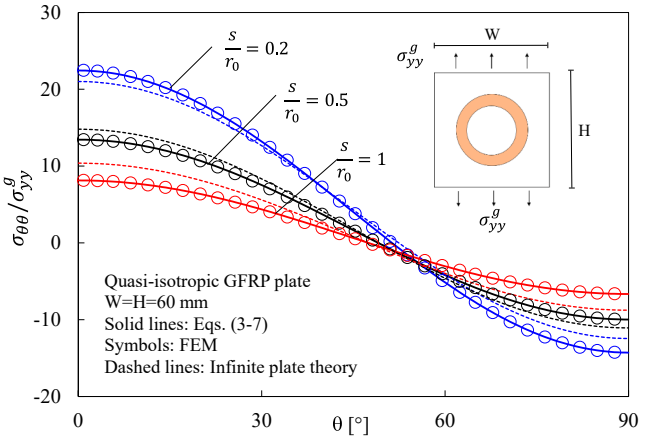

Fig. 6. Stress component $\sigma_{\theta\theta}$ evaluated along the boundary of the hole (path 4 in Fig. 5). 60 × 60 mm isotropic plates made of quasi-isotropic GFRP; hole radius $r_0 = 10$ mm reinforced with rings of width s = 2, 5 and 10 mm. Applied load according to load case L1. Analytical solution compared with the results from FE analyses and infinite plate theory.

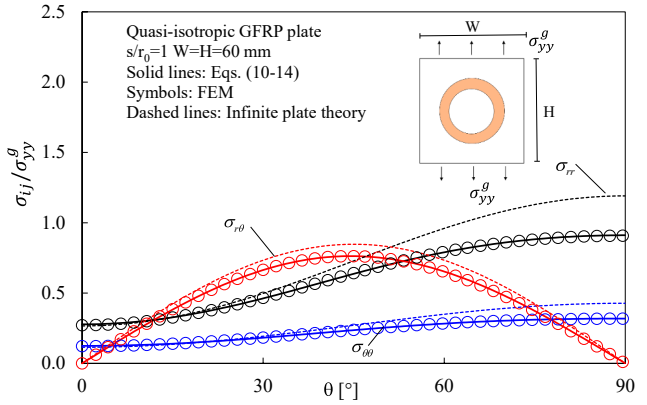

Fig. 7. Stress components σ_{rr}, $\sigma_{\theta\theta}$, $\sigma_{r\theta}$ evaluated along the edge of the reinforcing ring (path 5 in Fig. 5) in the plate material. P = 10; 60 × 60 mm plates made of quasi-isotropic GFRP; hole radius $r_0 = 10$ mm reinforced with a ring of width s = 10 mm. Applied load according to load case L1. Analytical solution compared with the results from FE analyses and infinite plate theory.

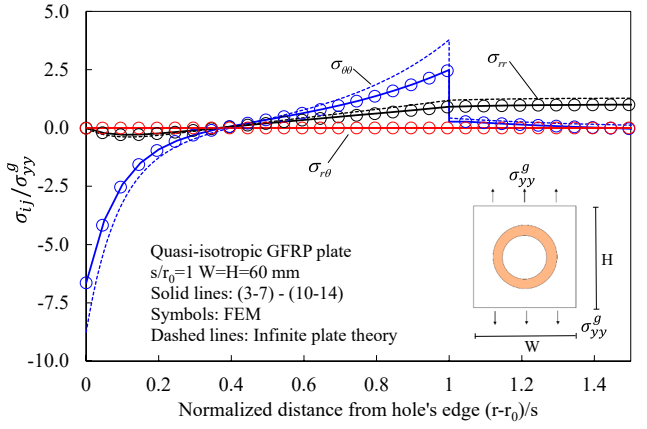

Fig. 8. Stress components σ_{rr}, $\sigma_{\theta\theta}$, $\sigma_{r\theta}$ evaluated along a straight path with θ = 90° (path 3 in Fig. 5). P = 10; 60 × 60 mm plates made of quasi-isotropic GFRP; hole radius $r_0 = 10$ mm reinforced with a ring of width s = 10 mm. Applied load according to load case L1. Analytical solution compared with the results from FE analyses and infinite plate theory.

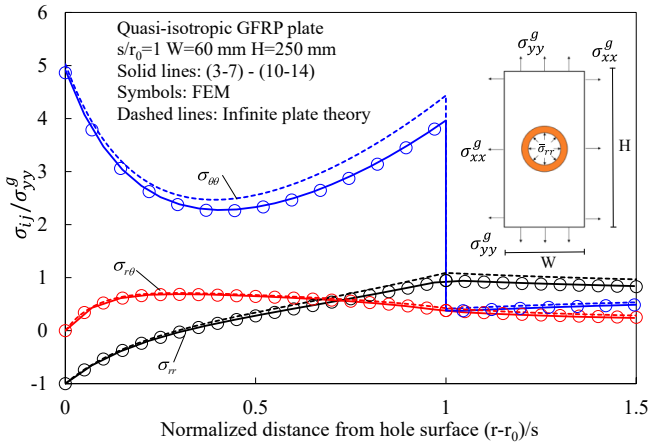

Fig. 9. Stress components σ_{rr}, $\sigma_{\theta\theta}$, $\sigma_{r\theta}$ evaluated along a straight path with θ = 45° (path 2 in Fig. 5). P = 10; 60 × 250 mm plates made of quasi-isotropic GFRP; hole radius $r_0 = 10$ mm reinforced with a ring of width s = 10 mm. Applied load according to load case L2. Analytical solution compared with the results from FE analyses and infinite plate theory.

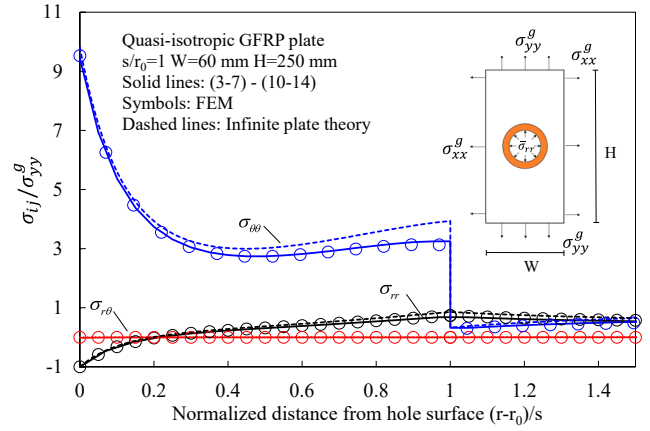

Fig. 10. Stress components σ_{rr}, $\sigma_{\theta\theta}$, $\sigma_{r\theta}$ evaluated along a straight path with θ = 0° (path 1 in Fig. 5). P = 10; 60 × 250 mm plates made of quasi-isotropic GFRP; hole radius $r_0 = 10$ mm reinforced with a ring of width s = 10 mm. Applied load according to load case L2. Analytical solution compared with the results from FE analyses and infinite plate theory.

$$\bar{\sigma}_{rr}(\theta) = \Phi(\theta) = \frac{100}{\pi} + 50\sin[\theta] - \frac{200\cos[2\theta]}{3\pi} - \frac{40\cos[4\theta]}{3\pi} - \frac{40\cos[6\theta]}{7\pi} - \frac{200\cos[8\theta]}{63\pi} - \frac{200\cos[10\theta]}{99\pi} \tag{35}$$

4. **L4**: biaxial tension–compression, with $\sigma^g_{yy} = 100\,MPa$ and $\sigma^g_{xx} = -50MPa$.
5. **L5**: biaxial tension–compression, with $\sigma^g_{yy} = 100\,MPa$ and $\sigma^g_{xx} = -50MPa$, and non-uniform internal pressure as per Eq. (35).
6. **L6**: harmonic load. With the following expressions:
   a. Pressure applied on the hole boundary as per Eq. (35).
   b. Tension applied on the lateral left and right edges as: $100\sin(4\theta)$.
   c. Tension applied to the upper and lower edges as: $100\sin[2(\theta - \pi/4)]$.
7. **L7**: harmonic load. With the following expressions:
   a. Pressure applied on the hole boundary as per Eq. (35).
   b. Tension applied on the lateral edges as: $100[\sin(4\theta) + \sin(8\theta)]$.

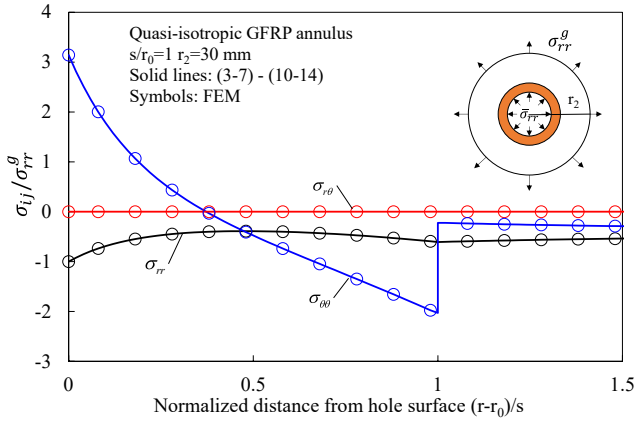

Fig. 11. Stress components σ_{rr}, $\sigma_{\theta\theta}$, $\sigma_{r\theta}$ evaluated along a straight path with $\theta = 45°$ (path 2 in Fig. 5). Quasi-isotropic GFRP annulus of external radius $r_2 = 30$ mm internal radius $r_0 = 10$ mm reinforced with a ring of width $s = 10$ mm. Applied loads: external radial tension ($\bar{\sigma}^g_{rr} = 100\,MPa$) and internal pressure ($\bar{\sigma}_{rr} = -100\,MPa$). Analytical solution compared with the results from FE analyses.

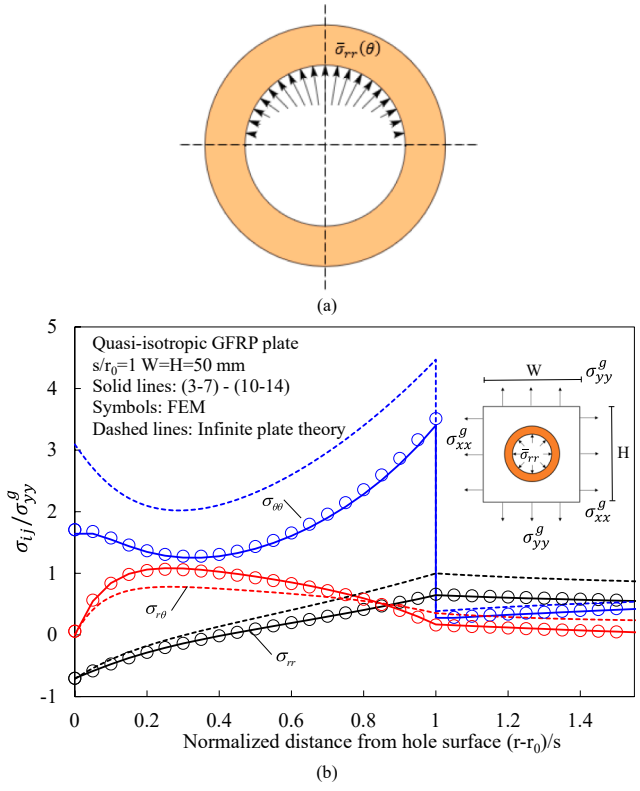

Fig. 12. (a) Schematic of the internal pressure exerted by a pin, according to the Eq. (35). (b) Stress components σ_{rr}, $\sigma_{\theta\theta}$, $\sigma_{r\theta}$ evaluated along a straight path with $\theta = 45°$ (path 2 in Fig. 3). P = 10; 50 × 50 mm plates made of quasi-isotropic GFRP; hole radius $r_0 = 10$ mm reinforced with a ring of width $s = 10$ mm. Applied load according to load case L3, non-uniform internal pressure according to Eq. (35) (see also Fig. 12a). Analytical solution compared with the results from FE analyses and infinite plate theory.

c. Tension applied to the upper and lower edges as: $100\{\sin[2(\theta - \pi/4)] + \sin[4(\theta - \pi/4)]\}$.

In all the analysed plates the annular reinforcement was chosen as made of Carbon Fibre Reinforced Polymer (CFRP) with the following elastic properties: $E_\theta = 147$ GPa, $E_r = 10.3$ GPa, $G_{\theta r} = 7$ GPa, $\nu_{r\theta} = 0.02$.

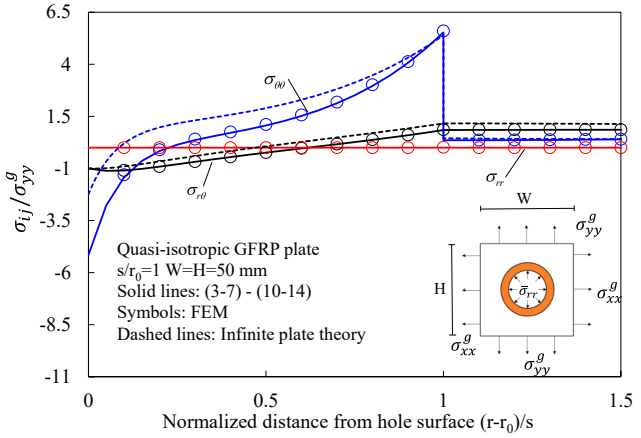

Fig. 13. Stress components σ_{rr}, $\sigma_{\theta\theta}$, $\sigma_{r\theta}$ evaluated along a straight path with $\theta = 90°$ (path 3 in Fig. 5). P = 10; 50 × 50 mm plates made of quasi-isotropic GFRP; hole radius $r_0 = 10$ mm reinforced with a ring of width $s = 10$ mm. Applied load according to load case L3. Analytical solution compared with the results from FE analyses and infinite plate theory.

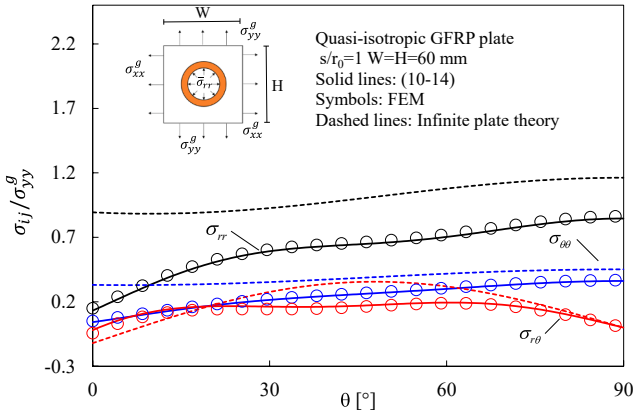

Fig. 14. Stress components σ_{rr}, $\sigma_{\theta\theta}$, $\sigma_{r\theta}$ evaluated along the edge of the reinforcing ring (path 5 in Fig. 5) in the matrix. 60 × 60 mm plates made of quasi-isotropic GFRP; hole radius $r_0 = 10$ mm reinforced with a ring of width $s = 10$ mm. Applied load according to load case L5. Analytical solution compared with the results from FE analyses and infinite plate theory.

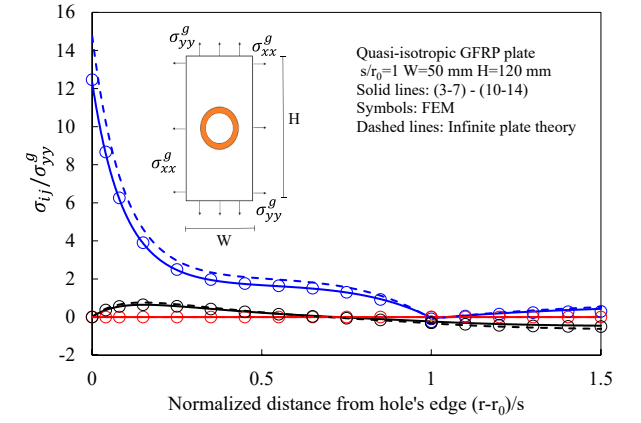

Fig. 15. Stress components σ_{rr}, $\sigma_{\theta\theta}$, $\sigma_{r\theta}$ evaluated along a straight path with $\theta = 0°$ (path 1 in Fig. 5). P = 14; 50 × 120 mm plates made of quasi-isotropic GFRP; hole radius r0 = 10 mm reinforced with a ring of width $s = 10$ mm. Applied load according to load case L4. Analytical solution compared with the results from FE analyses and infinite plate theory.

Differently, plates were made of quasi-isotropic Glass Fiber Reinforced Polymer (GFRP) laminate, with the following elastic properties: $E_x = E_y = 54$ GPa, and $\nu_{12} = \nu_{21} = 0.31$. In all the considered cases the hole diameter was 10 mm.

The model results are evaluated in terms of $\sigma_{\theta\theta}$ and compared with the results of FE analyses carried out with Ansys® version 21 software package, using Ansys PLANE183 quadrilateral plane elements under plane stress condition and pure displacement formulation. The mesh patterns were made following the same procedure reported in [30] assuring reliable FE results. The following parameter was used for assessing the accuracy of the analytical model:

$$\Delta = \left\| \frac{\sigma_{\theta\theta} - \sigma_{\theta\theta,FE}}{\sigma_{\theta\theta,FE}} \right\| = \|\mathrm{var}(\sigma_{\theta\theta})\| \tag{36}$$

where $\sigma_{\theta\theta}$ is the stress value predicted by the semi-analytical solution proposed in this article, and $\sigma_{\theta\theta,FE}$ is the stress value obtained from the numerical analysis.

The stresses from numerical analyses were evaluated in Points P1, P2, and P3 (regarded as representative of the stress field for the purpose of studying the solution convergence; see Table 1 and Fig. 1) and compared with theoretical predictions (see Figs. 2, 3 and 4).

Considering point P1 in Fig. 2, the convergence is fast, and at 10 Fourier terms the deviation is below 5 % in all the considered scenarios. Differently, point P2 in Fig. 3 exhibits a lower convergence, especially for r_1 of 20 mm, and load case L4 seems to be the most affected by this behaviour. Eventually, considering point P3 in Fig. 4 the trend is similar to that of point P2.

Regardless of the load case, or the plate and annulus size, adding more terms to the Fourier series the stress values converge to asymptotic values. Yet, the annulus size and the plate aspect ratio affect the convergence speed, as much as the point that is being investigated. Convergence seems to be affected by the load case, as well, but marginally if compared with the previous parameters.

The outcome of the convergence analysis is reasonable: as with all the methodologies that employ numerical approximations over a geometrical domain, whenever the domain presents relevant differences among its dimensions, the numerical calculus is less accurate.

At the same time, the fact that the load case is less important as compared to the geometrical dimensions is a consequence of the way in which the model makes use of Fourier approximations: the application of constant, or non-constant, loadings does not affect the way in which the model maps those conditions to its potential formulations. Generally, in the case of a squared plate, one can reach an acceptable overall precision using as much terms in the Fourier expansions as the highest degree used to describe the applied loads in (1) and (2) with a minimum of 5. For rectangular plates instead, the accuracy of the results is less predictable and a general rule that can cover all the aspect ratios and load cases cannot be provided *a priori*; for these cases, a convergence analysis is recommended.

4.2. Stress fields comparisons

The previous section investigated the deviations in convergence, but it did not provide a reference to the absolute value of the stresses in those investigated points: high errors in a region with low stresses could still be acceptable, thus it is important to evaluate the actual stress values and not just their errors. To shed light on this aspect, in this Section the comparison between the model predictions and the FE results are reported directly in terms of stresses along several path in selected cases. In addition, the results are compared with the prediction of the previous model for the case of infinite plates [30], in order to make it explicit the improved accuracy of the new solution.

The analyzed plates had a central hole of radius $r_0 = 10$ mm, width varying between 50 and 60 mm, height varying between 50 and 250 mm, and were reinforced with annuli of thickness equal to $s = 2$, 5 and 10 mm. Stresses were evaluated along 5 paths according to Fig. 5, with 3 straight paths starting from the centre of the hole and inclined along the $\theta = 0°$, 45° and 90° directions (paths 1, 2 and 3, respectively), one path along the hole boundary (path 4) and the last one along the boundary of the reinforcing region (path 5). Analysed loading conditions include uniaxial tension, biaxial tension, and uniform and non-uniform internal pressure. The materials used in the FE analyses are the same as those used in the convergence analyses and the number of terms for the Fourier expansions used for the analytical evaluations are in all cases 10, in accordance with the convergence analysis, targeting an overall error of less than 5 %. Comparisons between analytical and numerical analyses are shown in Figs. 6–15 along with the results from the infinite plate model derived in [30]. In all the discussed cases the agreement between the proposed model and numerical analyses is excellent. Additional comparisons with the exact solution developed for the infinite plate [30] were carried out, to provide more information about the approximations introduced when dealing with plates characterized by holes relatively big with respect to the plate size. In more detail, for the infinite plate theory solution the hoop stress is again severely affected by the finiteness of the plate. Accordingly, for practical engineering application of finite size bodies the solution presented in this manuscript offers a better modelling of the plate stress and displacement fields than the closed-form solution presented in [30], thus justifying the additional efforts needed to address this problem.

In Fig. 6 the hoop stress component is shown as evaluated along the boundary of the hole for 60 × 60 mm^2 plates under uniaxial tension, considering 3 different thickness values of the reinforced annulus. It is evident how the infinite plate theory either underestimates or overestimates stress concentrations depending on the configuration, while the proposed model perfectly approximates the stress fields along the hole boundary.

Taking as a reference the 60 × 60 mm^2 plate with $s/r_0 = 1$ under the same loading conditions, in Figs. 7 and 8 stresses along the boundary of the reinforced region (path 5) and along path 3 are shown, according to which, conclusions similar to those related to Fig. 6 can be drawn. Remarkable are the results for the radial stress of Fig. 7 and for the hoop stress of Fig. 8, where the model for infinite plate overestimates the stress concentration by almost 30 %.

Figs. 9 and 10 show the stress components for a 60x250 mm^2 rectangular plate with $s/r_0 = 1$, under a biaxial tension and internal constant pressure. Stresses were calculated along path 2 (Fig. 9) and path 1 (Fig. 10). Also for these cases, the accuracy of the proposed solution is remarkable.

Fig. 11 deals with the special case of a circular plate with a central hole (see Section 3) under external tension and internal pressure, showing that in this particular case the proposed formulation gives an exact solution and that the results are in perfect agreement with numerical analyses.

Figs. 12–14 instead investigate some cases of non-constant loadings, particularly assuming as internal pressure that exerted by a pin, as per Eq. (35).

Fig. 15 is intended to show that the convergence analysis done in the previous chapter can show very high relative errors in the stresses calculated at one point, and nonetheless be an extremely good approximation of the overall stress fields. Referring to Fig. 3, taking as an example the case of load case L4 and angular stresses calculated in P2 for a 50 × 120 mm plate with a reinforcing annulus of width 10 mm, the relative error reaches 75 %. In Fig. 15 the stress components along path 1 are plotted, and it is shown how the predicted stresses are in excellent accordance with the finite element analysis, and the 75 % error at the normalized distance $(r\text{-}r_0)/s = 1$ is mainly due to the fact that the

normalized stresses in that point are close to null.

In all the discussed cases the agreement between the proposed model and numerical analyses is excellent, showing significant improvements compared to the infinite plate theory. In more detail, for the latter solution the hoop stress is again severely affected by the finiteness of the plate. Accordingly, for practical engineering application of finite size bodies the solution presented in this manuscript offers a better modelling of the plate stress and displacement fields than the closed-form solution presented in [30], thus justifying the additional efforts needed to address this problem.

5. Conclusions

In this work an approximate solution was proposed for a finite plate with a circular hole reinforced with a polarly orthotropic material and a generic loading condition. The derived solution for displacements and stress fields, although not exact, is extremely accurate for all the possible plane loadings as well as geometric parameters of the problem. The solution was tested against a bulk of finite element analyses carried out on different combinations of geometrical and loading parameters and found to be extremely satisfactory in all cases. It was also shown how the solution can easily accommodate complex loading conditions with arbitrary precision while relying on a stable convergence of the numerical method proposed.

The solution presented in this paper can be regarded as a valuable contribution to the toolset of material designers charged with the challenging task of handling the additional degrees of freedom offered by additive manufacturing technology applied to the field of composite materials.

Declaration of Competing Interest

The authors declare that they have no known competing financial interests or personal relationships that could have appeared to influence the work reported in this paper.

Data availability

Data will be made available on request.

Acknowledgements

Michele Zappalorto would like to acknowledge the financial support from the University of Padova within the research project BIRD215331/21, "*Analysis and modelling of Advanced Structural Composites made by Additive Manufacturing*".

Appendix A

Let's introduce the following constants:

$$\xi = \frac{d^2-\epsilon^2}{d^2\left(1+\epsilon^2\right)};\qquad \zeta = \frac{\left(1+d^2\right)\epsilon^2}{d^2\left(1+\epsilon^2\right)};\qquad \delta = \frac{1}{c^2}-\frac{\left(1+d^2\right)\epsilon^2}{d^4\left(1+\epsilon^2\right)};$$
$$\eta = \frac{1}{d^2}-\frac{\alpha_0}{c^2};\qquad \varrho = \frac{1}{d^2}+\frac{\alpha_0}{c^2};\tag{A.1}$$
$$g_{\gamma,n} = \frac{n+\phi_{\gamma,n}}{d^2}-\frac{\gamma\phi_{\gamma,n}}{c^2};\quad f_{\gamma,n} = 1+\gamma+n\phi_{\gamma,n};$$

$$\widehat{\mathbf{H}}_0 = \begin{bmatrix} \eta\frac{r_0^{\alpha_0}}{r_1^{1+\alpha_0}}G_{\theta r}^{(1)} & \frac{\varrho G_{\theta r}^{(1)}}{r_1} & -\frac{1}{r_1^2} & 0 & 0 & 0 \\ \frac{\eta G_{\theta r}^{(1)}}{r_1} & \varrho\frac{r_0^{\alpha_0}}{r_0 r_1^{\alpha_0}}G_{\theta r}^{(1)} & 0 & 0 & 0 & 0 \\ \frac{r_0^{\alpha_0}}{r_1^{\alpha_0}} & 1 & \frac{1+\nu^{(2)}}{E^{(2)}r_1} & 0 & 0 & 0 \\ 0 & 0 & 0 & \frac{1}{r_1^2} & \frac{2r_0 G_{\theta r}^{(1)}}{r_1^2} & 0 \\ 0 & 0 & 0 & -\frac{1+\nu^{(2)}}{E^{(2)}r_1} & -\frac{r_0}{r_1} & -\frac{4r_1}{E^{(2)}} \\ 0 & 0 & 0 & 0 & \frac{2G_{\theta r}^{(1)}}{r_0} & 0 \end{bmatrix}\tag{A.2}$$

$$\widehat{\mathbf{H}}_n = \begin{bmatrix} \widehat{\mathbf{H}}_{n,1} & \widehat{0} \\ \widehat{0} & \widehat{\mathbf{H}}_{n,2} \end{bmatrix}\tag{A.3}$$

where $\widehat{0}$ are 6x6 null matrices and:

$$\widehat{\mathbf{H}}_{1,1} = \begin{bmatrix} \frac{r_0^{\alpha_1}}{r_1^{1+\alpha_1}} g_{\alpha,1} G_{\theta r}^{(1)} & \frac{g_{-\alpha,1} G_{\theta r}^{(1)}}{r_1} & \frac{\delta G_{\theta r}^{(1)}}{r_1} & -\frac{2\left(\nu^{(2)}+3\right)}{r_1\left(1+\nu^{(2)}\right)} & -\frac{2}{r_1^3} & 0 \\ -\frac{r_0^{\alpha_1}}{r_1^{1+\alpha_1}} f_{\alpha,1} G_{\theta r}^{(1)} & -\frac{f_{-\alpha,1} G_{\theta r}^{(1)}}{r_1} & -\frac{\xi G_{\theta r}^{(1)}}{r_1} & \frac{2\left(1-\nu^{(2)}\right)}{r_1\left(1+\nu^{(2)}\right)} & -\frac{2}{r_1^3} & 0 \\ \frac{g_{\alpha,1} G_{\theta r}^{(1)}}{r_0} & \frac{r_0^{\alpha_1}}{r_0 r_1^{\alpha_1}} g_{-\alpha,1} G_{\theta r}^{(1)} & \frac{\delta G_{\theta r}^{(1)}}{r_0} & 0 & 0 & 0 \\ -\frac{f_{\alpha,1} G_{\theta r}^{(1)}}{r_0} & -\frac{r_0^{\alpha_1}}{r_0 r_1^{\alpha_1}} f_{-\alpha,1} G_{\theta r}^{(1)} & -\frac{\xi G_{\theta r}^{(1)}}{r_0} & 0 & 0 & 0 \\ \frac{r_0^{\alpha_1}}{r_1^{\alpha_1}} \phi_{\alpha,1} & \phi_{-\alpha,1} & \log\left[\frac{r_1}{r_0}\right] - \zeta & \frac{1+\nu^{(2)}+2\left(\nu^{(2)}-3\right)\log[r_1]}{E^{(2)}} & \frac{1+\nu^{(2)}}{E^{(2)} r_1^2} & \frac{\nu^{(2)}-3}{E^{(2)}} \\ \frac{r_0^{\alpha_1}}{r_1^{\alpha_1}} & 1 & -\log\left[\frac{r_1}{r_0}\right] & \frac{1+\nu^{(2)}-2\left(\nu^{(2)}-3\right)\log[r_1]}{E^{(2)}} & \frac{1+\nu^{(2)}}{E^{(2)} r_1^2} & \frac{3-\nu^{(2)}}{E^{(2)}} \end{bmatrix} \tag{A.4}$$

$$\widehat{\mathbf{H}}_{1,2} = \begin{bmatrix} \frac{r_0^{\alpha_1}}{r_1^{1+\alpha_1}} g_{\alpha,1} G_{\theta r}^{(1)} & \frac{g_{-\alpha,1} G_{\theta r}^{(1)}}{r_1} & \frac{\delta G_{\theta r}^{(1)}}{r_1} & -\frac{2\left(\nu^{(2)}+3\right)}{r_1\left(1+\nu^{(2)}\right)} & -\frac{2}{r_1^3} & 0 \\ \frac{r_0^{\alpha_1}}{r_1^{1+\alpha_1}} f_{\alpha,1} G_{\theta r}^{(1)} & \frac{f_{-\alpha,1} G_{\theta r}^{(1)}}{r_1} & \frac{\xi G_{\theta r}^{(1)}}{r_1} & \frac{2\left(\nu^{(2)}-1\right)}{r_1\left(1+\nu^{(2)}\right)} & \frac{2}{r_1^3} & 0 \\ \frac{g_{\alpha,1} G_{\theta r}^{(1)}}{r_0} & \frac{r_0^{\alpha_1}}{r_0 r_1^{\alpha_1}} g_{-\alpha,1} G_{\theta r}^{(1)} & \frac{\delta G_{\theta r}^{(1)}}{r_0} & 0 & 0 & 0 \\ \frac{f_{\alpha,1} G_{\theta r}^{(1)}}{r_0} & \frac{r_0^{\alpha_1}}{r_0 r_1^{\alpha_1}} f_{-\alpha,1} G_{\theta r}^{(1)} & \frac{\xi G_{\theta r}^{(1)}}{r_0} & 0 & 0 & 0 \\ \frac{r_0^{\alpha_1}}{r_1^{\alpha_1}} \phi_{\alpha,1} & \phi_{-\alpha,1} & \log\left[\frac{r_1}{r_0}\right] & \frac{1+\nu^{(2)}+2\left(\nu^{(2)}-3\right)\log[r_1]}{E^{(2)}} & \frac{1+\nu^{(2)}}{E^{(2)} r_1^2} & \frac{\nu^{(2)}-3}{E^{(2)}} \\ -\frac{r_0^{\alpha_1}}{r_1^{\alpha_1}} & -1 & \zeta + \log\left[\frac{r_1}{r_0}\right] & -\frac{1+\nu^{(2)}-2\left(\nu^{(2)}-3\right)\log[r_1]}{E^{(2)}} & -\frac{1+\nu^{(2)}}{E^{(2)} r_1^2} & \frac{\nu^{(2)}-3}{E^{(2)}} \end{bmatrix} \tag{A.5}$$

$$\widehat{\mathbf{H}}_{n,1} = \begin{bmatrix} \frac{r_0^{\alpha_n}}{r_1^{1+\alpha_n}} g_{\alpha,n} G_{\theta r}^{(1)} & \frac{r_0^{\beta_n}}{r_1^{1+\beta_n}} g_{\beta,n} G_{\theta r}^{(1)} & \frac{g_{-\alpha,n} G_{\theta r}^{(1)}}{r_1} & \frac{g_{-\beta,n} G_{\theta r}^{(1)}}{r_1} & \frac{n^2+n-2}{r_1^n} & -\frac{n+1}{r_1^{n+2}} \\ -\frac{r_0^{\alpha_n}}{r_1^{1+\alpha_n}} f_{\alpha,n} G_{\theta r}^{(1)} & -\frac{r_0^{\beta_n}}{r_1^{1+\beta_n}} f_{\beta,n} G_{\theta r}^{(1)} & -\frac{f_{-\alpha,n} G_{\theta r}^{(1)}}{r_1} & -\frac{f_{-\beta,n} G_{\theta r}^{(1)}}{r_1} & \frac{n^2-n}{r_1^n} & -\frac{n+1}{r_1^{n+2}} \\ \frac{g_{\alpha,n} G_{\theta r}^{(1)}}{r_0} & \frac{g_{\beta,n} G_{\theta r}^{(1)}}{r_0} & \frac{r_0^{\alpha_n}}{r_0 r_1^{\alpha_n}} g_{-\alpha,n} G_{\theta r}^{(1)} & \frac{r_0^{\beta_n}}{r_0 r_1^{\beta_n}} g_{-\beta,n} G_{\theta r}^{(1)} & 0 & 0 \\ -\frac{f_{\alpha,n} G_{\theta r}^{(1)}}{r_0} & -\frac{f_{\beta,n} G_{\theta r}^{(1)}}{r_0} & -\frac{r_0^{\alpha_n}}{r_0 r_1^{\alpha_n}} f_{-\alpha,n} G_{\theta r}^{(1)} & -\frac{r_0^{\beta_n}}{r_0 r_1^{\beta_n}} f_{-\beta,n} G_{\theta r}^{(1)} & 0 & 0 \\ \frac{r_0^{\alpha_n}}{r_1^{\alpha_n}} \phi_{\alpha,n} & \frac{r_0^{\beta_n}}{r_1^{\beta_n}} \phi_{\beta,n} & \phi_{-\alpha,n} & \phi_{-\beta,n} & -\frac{n+2+(n-2)\nu^{(2)}}{E^{(2)} r_1^{n-1}} & \frac{\nu^{(2)}+1}{E^{(2)} r_1^{n+1}} \\ \frac{r_0^{\alpha_n}}{r_1^{\alpha_n}} & \frac{r_0^{\beta_n}}{r_1^{\beta_n}} & 1 & 1 & -\frac{n-4+n\nu^{(2)}}{E^{(2)} r_1^{n-1}} & \frac{\nu^{(2)}+1}{E^{(2)} r_1^{n+1}} \end{bmatrix} \tag{A.6}$$

$$\widehat{\mathbf{H}}_{n,2} = \begin{bmatrix} \frac{r_0^{\alpha_n}}{r_1^{1+\alpha_n}} g_{\alpha,n} G_{\theta r}^{(1)} & \frac{r_0^{\beta_n}}{r_1^{1+\beta_n}} g_{\beta,n} G_{\theta r}^{(1)} & \frac{g_{-\alpha,n} G_{\theta r}^{(1)}}{r_1} & \frac{g_{-\beta,n} G_{\theta r}^{(1)}}{r_1} & \frac{n^2+n-2}{r_1^n} & -\frac{n+1}{r_1^{n+2}} \\ \frac{r_0^{\alpha_n}}{r_1^{1+\alpha_n}} f_{\alpha,n} G_{\theta r}^{(1)} & \frac{r_0^{\beta_n}}{r_1^{1+\beta_n}} f_{\beta,n} G_{\theta r}^{(1)} & \frac{f_{-\alpha,n} G_{\theta r}^{(1)}}{r_1} & \frac{f_{-\beta,n} G_{\theta r}^{(1)}}{r_1} & -\frac{n^2-n}{r_1^n} & \frac{n+1}{r_1^{n+2}} \\ \frac{g_{\alpha,n} G_{\theta r}^{(1)}}{r_0} & \frac{g_{\beta,n} G_{\theta r}^{(1)}}{r_0} & \frac{r_0^{\alpha_n}}{r_0 r_1^{\alpha_n}} g_{-\alpha,n} G_{\theta r}^{(1)} & \frac{r_0^{\beta_n}}{r_0 r_1^{\beta_n}} g_{-\beta,n} G_{\theta r}^{(1)} & 0 & 0 \\ \frac{f_{\alpha,n} G_{\theta r}^{(1)}}{r_0} & \frac{f_{\beta,n} G_{\theta r}^{(1)}}{r_0} & \frac{r_0^{\alpha_n}}{r_0 r_1^{\alpha_n}} f_{-\alpha,n} G_{\theta r}^{(1)} & \frac{r_0^{\beta_n}}{r_0 r_1^{\beta_n}} f_{-\beta,n} G_{\theta r}^{(1)} & 0 & 0 \\ \frac{r_0^{\alpha_n}}{r_1^{\alpha_n}} \phi_{\alpha,n} & \frac{r_0^{\beta_n}}{r_1^{\beta_n}} \phi_{\beta,n} & \phi_{-\alpha,n} & \phi_{-\beta,n} & -\frac{n+2+(n-2)\nu^{(2)}}{E^{(2)} r_1^{n-1}} & \frac{\nu^{(2)}+1}{E^{(2)} r_1^{n+1}} \\ -\frac{r_0^{\alpha_n}}{r_1^{\alpha_n}} & -\frac{r_0^{\beta_n}}{r_1^{\beta_n}} & -1 & -1 & \frac{n-4+n\nu^{(2)}}{E^{(2)} r_1^{n-1}} & -\frac{\nu^{(2)}+1}{E^{(2)} r_1^{n+1}} \end{bmatrix} \tag{A.7}$$

For $2 \le n \le P$

$$\bar{k} = \{\bar{k}_0, \bar{k}_1, \cdots, \bar{k}_N\} \tag{A.9}$$

$$\bar{k}_0 = \left\{ -2\bar{A}_1, -S_0, \frac{2\left(\nu^{(2)}-1\right)r_1\bar{A}_1}{E^{(2)}}, 0, 0, -T_0 \right\} \tag{A.10}$$

$$\bar{k}_1 = \begin{Bmatrix} -2r_1\bar{A}_2 \\ -2r_1\bar{A}_2 \\ -S_{1,1} \\ -T_{1,2} \\ \frac{\left(3\nu^{(2)}-1\right)r_1^2\bar{A}_2}{E^{(2)}} \\ -\frac{\left(5+\nu^{(2)}\right)r_1^2\bar{A}_2}{E^{(2)}} \\ 2r_1\bar{B}_2 \\ -2r_1\bar{B}_2 \\ -S_{1,2} \\ -T_{1,1} \\ \frac{\left(3\nu^{(2)}-1\right)r_1^2\bar{B}_2}{E^{(2)}} \\ -\frac{\left(5+\nu^{(2)}\right)r_1^2\bar{B}_2}{E^{(2)}} \end{Bmatrix}; \bar{k}_n = \begin{Bmatrix} \left(n^2-n-2\right)r_1^n\bar{A}_{n+1} + (n-1)r_1^{n-2}\bar{C}_{n-1} \\ -\left(n^2+n\right)r_1^n\bar{A}_{n+1} - (n-1)r_1^{n-2}\bar{C}_{n-1} \\ -S_{n,1} \\ -T_{n,2} \\ \frac{\left(n-2+(n+2)\nu^{(2)}\right)r_1^{n+1}\bar{A}_{n+1} + r_1^{n-1}\left(1+\nu^{(2)}\right)\bar{C}_{n-1}}{E^{(2)}} \\ -\frac{\left(2n-1+n\nu^{(2)}\right)r_1^{n+1}\bar{A}_{n+1} + r_1^{n-1}\left(1+\nu^{(2)}\right)\bar{C}_{n-1}}{E^{(2)}} \\ -\left(n^2-n-2\right)r_1^n\bar{B}_{n+1} - (n-1)r_1^{n-2}\bar{D}_{n-1} \\ -\left(n^2+n\right)r_1^n\bar{B}_{n+1} - (n-1)r_1^{n-2}\bar{D}_{n-1} \\ -S_{n,2} \\ -T_{n,1} \\ -\frac{\left(n-2+(n+2)\nu^{(2)}\right)r_1^{n+1}\bar{B}_{n+1} + r_1^{n-1}\left(1+\nu^{(2)}\right)\bar{D}_{n-1}}{E^{(2)}} \\ -\frac{\left(2n-1+n\nu^{(2)}\right)r_1^{n+1}\bar{B}_{n+1} + r_1^{n-1}\left(1+\nu^{(2)}\right)\bar{D}_{n-1}}{E^{(2)}} \end{Bmatrix} \tag{A.11}$$

Appendix B

$$\widehat{\mathbf{H}}_0^* = \begin{bmatrix} \eta\frac{r_0^{\alpha_0}}{r_1^{1+\alpha_0}}G_{\theta r}^{(1)} & \rangle\frac{G_{\theta r}^{(1)}}{r_1} & -\frac{1}{\rho 2^2} & \frac{(\kappa-1)\left(1+\nu^{(2)}\right)}{\nu^{(2)}-1} & 0 & 0 & 0 \\ \frac{r_0^{\alpha_0}}{r_1^{\alpha_0}} & 1 & \frac{1+\nu^{(2)}}{E^{(2)}r_1} & \frac{(1-\kappa)\left(1+\nu^{(2)}\right)r_1}{E^{(2)}} & 0 & 0 & 0 \\ \frac{\eta G_{\theta r}^{(1)}}{r_1} & \rangle\frac{r_0^{\alpha_0}}{r_0 r_1^{\alpha_0}}G_{\theta r}^{(1)} & 0 & 0 & 0 & 0 & 0 \\ 0 & 0 & \frac{1}{r_2^2} & \frac{(1-\kappa)\left(1+\nu^{(2)}\right)}{\nu^{(2)}-1} & 0 & 0 & 0 \\ 0 & 0 & 0 & 0 & \frac{1}{r_1^2} & \frac{2r_0G_{\theta r}^{(1)}}{r_1^2} & 0 \\ 0 & 0 & 0 & 0 & -\frac{1+\nu^{(2)}}{E^{(2)}r_1} & -\frac{r_0}{r_1} & -\frac{(\kappa+1)\left(1+\nu^{(2)}\right)r_1}{E^{(2)}} \\ 0 & 0 & 0 & 0 & 0 & \frac{2G_{\theta r}^{(1)}}{r_0} & 0 \end{bmatrix} \tag{B.1}$$

$$\widehat{\mathbf{H}}_n^* = \begin{bmatrix} \widehat{\mathbf{H}}_{n,1}^* & \widehat{0} \\ \widehat{0} & \widehat{\mathbf{H}}_{n,2}^* \end{bmatrix} \tag{B.2}$$

$$\widehat{\mathbf{H}}^{*}_{1,1}=\begin{bmatrix}
\frac{r_0^{\alpha_1}}{r_1^{1+\alpha_1}}g_{\alpha,1}G^{(1)}_{\theta r} & \frac{g_{-\alpha,1}G^{(1)}_{\theta r}}{r_1} & \frac{\delta G^{(1)}_{\theta r}}{r_1} & \frac{2\left(\kappa-\nu^{(2)}\right)}{\left(\nu^{(2)}-1\right)r_1} & -\frac{2}{r_1^3} & 0 & \frac{2\left(\kappa+\kappa\nu^{(2)}-2\right)r_1}{\nu^{(2)}-1}\\
-\frac{r_0^{\alpha_1}}{r_1^{1+\alpha_1}}f_{\alpha,1}G^{(1)}_{\theta r} & -\frac{f_{-\alpha,1}G^{(1)}_{\theta r}}{r_1} & -\frac{\xi G^{(1)}_{\theta r}}{r_1} & \frac{\kappa-1}{r_1} & -\frac{2}{r_1^3} & 0 & -2r_1\\
\frac{g_{\alpha,1}G^{(1)}_{\theta r}}{r_0} & \frac{r_0^{\alpha_1}}{r_0r_1^{\alpha_1}}g_{-\alpha,1}G^{(1)}_{\theta r} & \frac{\delta G^{(1)}_{\theta r}}{r_0} & 0 & 0 & 0 & 0\\
-\frac{f_{\alpha,1}G^{(1)}_{\theta r}}{r_0} & -\frac{r_0^{\alpha_1}}{r_0r_1^{\alpha_1}}f_{-\alpha,1}G^{(1)}_{\theta r} & -\frac{\xi G^{(1)}_{\theta r}}{r_0} & 0 & 0 & 0 & 0\\
\frac{r_0^{\alpha_1}}{r_1^{\alpha_1}}\phi_{\alpha,1} & \phi_{-\alpha,1} & \log\left[\frac{r_1}{r_0}\right]-\zeta & -\frac{\left(1+\nu^{(2)}\right)\left(\kappa\log\left[r_1^2\right]-1\right)}{E^{(2)}} & \frac{1+\nu^{(2)}}{E^{(2)}r_1^2} & -\frac{\kappa\left(1+\nu^{(2)}\right)}{E^{(2)}} & -\frac{(\kappa-2)\left(1+\nu^{(2)}\right)r_1^2}{E^{(2)}}\\
\frac{r_0^{\alpha_1}}{r_1^{\alpha_1}} & 1 & -\log\left[\frac{r_1}{r_0}\right] & -\frac{\left(1+\nu^{(2)}\right)\left(\kappa\log\left[r_1^2\right]+1\right)}{E^{(2)}} & \frac{1+\nu^{(2)}}{E^{(2)}r_1^2} & \frac{\kappa\left(1+\nu^{(2)}\right)}{E^{(2)}} & -\frac{(2+\kappa)\left(1+\nu^{(2)}\right)r_1^2}{E^{(2)}}\\
0 & 0 & 0 & \frac{2\left(\kappa-\nu^{(2)}\right)}{r_2\left(1-\nu^{(2)}\right)} & \frac{2}{r_2^3} & 0 & -\frac{2\left(\kappa+\kappa\nu^{(2)}-2\right)r_2}{\nu^{(2)}-1}
\end{bmatrix} \tag{B.3}$$

$$\widehat{\mathbf{H}}^{*}_{1,2}=\begin{bmatrix}
\frac{r_0^{\alpha_1}}{r_1^{1+\alpha_1}}g_{\alpha,1}G^{(1)}_{\theta r} & \frac{g_{-\alpha,1}G^{(1)}_{\theta r}}{r_1} & \frac{\delta G^{(1)}_{\theta r}}{r_1} & \frac{2\left(\kappa-\nu^{(2)}\right)}{\left(\nu^{(2)}-1\right)r_1} & -\frac{2}{r_1^3} & 0 & -\frac{2\left(\kappa+\kappa\nu^{(2)}-2\right)r_1}{\nu^{(2)}-1}\\
\frac{r_0^{\alpha_1}}{r_1^{1+\alpha_1}}f_{\alpha,1}G^{(1)}_{\theta r} & \frac{f_{-\alpha,1}G^{(1)}_{\theta r}}{r_1} & \frac{\xi G^{(1)}_{\theta r}}{r_1} & \frac{1-\kappa}{r_1} & -\frac{2}{r_1^3} & 0 & -2r_1\\
\frac{g_{\alpha,1}G^{(1)}_{\theta r}}{r_0} & \frac{r_0^{\alpha_1}}{r_0r_1^{\alpha_1}}g_{-\alpha,1}G^{(1)}_{\theta r} & \frac{\delta G^{(1)}_{\theta r}}{r_0} & 0 & 0 & 0 & 0\\
\frac{f_{\alpha,1}G^{(1)}_{\theta r}}{r_0} & \frac{r_0^{\alpha_1}}{r_0r_1^{\alpha_1}}f_{-\alpha,1}G^{(1)}_{\theta r} & \frac{\xi G^{(1)}_{\theta r}}{r_0} & 0 & 0 & 0 & 0\\
\frac{r_0^{\alpha_1}}{r_1^{\alpha_1}}\phi_{\alpha,1} & \phi_{-\alpha,1} & \log\left[\frac{r_1}{r_0}\right] & -\frac{\left(1+\nu^{(2)}\right)\left(\kappa\log\left[r_1^2\right]-1\right)}{E^{(2)}} & \frac{1+\nu^{(2)}}{E^{(2)}r_1^2} & -\frac{\kappa\left(1+\nu^{(2)}\right)}{E^{(2)}} & \frac{(\kappa-2)\left(1+\nu^{(2)}\right)r_1^2}{E^{(2)}}\\
-\frac{r_0^{\alpha_1}}{r_1^{\alpha_1}} & -1 & \zeta+\log\left[\frac{r_1}{r_0}\right] & -\frac{\left(1+\nu^{(2)}\right)\left(\kappa\log\left[r_1^2\right]+1\right)}{E^{(2)}} & -\frac{1+\nu^{(2)}}{E^{(2)}r_1^2} & -\frac{\kappa\left(1+\nu^{(2)}\right)}{E^{(2)}} & -\frac{(\kappa+2)\left(1+\nu^{(2)}\right)r_1^2}{E^{(2)}}\\
0 & 0 & 0 & \frac{2\left(\kappa-\nu^{(2)}\right)}{r_2\left(1-\nu^{(2)}\right)} & \frac{2}{r_2^3} & 0 & \frac{2\left(\kappa+\kappa\nu^{(2)}-2\right)r_2}{\nu^{(2)}-1}
\end{bmatrix} \tag{B.4}$$

$$\hat{\mathbf{H}}^{*}_{n,1}=\begin{bmatrix}
\frac{r_0^{\alpha_n}}{r_1^{1+\alpha_n}}g_{\alpha,n}G^{(1)}_{\theta r} & \frac{r_0^{\beta_n}}{r_1^{1+\beta_n}}g_{\beta,n}G^{(1)}_{\theta r} & \frac{g_{-\alpha,n}G^{(1)}_{\theta r}}{r_1} & \frac{g_{-\beta,n}G^{(1)}_{\theta r}}{r_1} & \frac{(1-n)\left((n-1)+\kappa+\left(\kappa-(n+1)\right)\nu^{(2)}\right)}{\left(\nu^{(2)}-1\right)r_1^{\,n}} & -\frac{(n+1)}{r_1^{\,n+2}} & \frac{(n+1)\left(\kappa+\left((n-1)+\kappa\right)\nu^{(2)}-(n+1)\right)r_1^{\,n}}{\left(\nu^{(2)}-1\right)} & (n-1)r_1^{\,n-2}\\
-\frac{r_0^{\alpha_n}}{r_1^{1+\alpha_n}}f_{\alpha,n}G^{(1)}_{\theta r} & -\frac{r_0^{\beta_n}}{r_1^{1+\beta_n}}f_{\beta,n}G^{(1)}_{\theta r} & -\frac{f_{-\alpha,n}G^{(1)}_{\theta r}}{r_1} & -\frac{f_{-\beta,n}G^{(1)}_{\theta r}}{r_1} & \frac{\left(n^2-n\right)}{r_1^{\,n}} & -\frac{(n+1)}{r_1^{\,n+2}} & -\left(n^2-n\right)r_1^{\,n} & -(n-1)r_1^{\,n-2}\\
\frac{g_{\alpha,n}G^{(1)}_{\theta r}}{r_0} & \frac{g_{\beta,n}G^{(1)}_{\theta r}}{r_0} & \frac{r_0^{\alpha_n}}{r_0r_1^{\alpha_n}}g_{-\alpha,n}G^{(1)}_{\theta r} & \frac{r_0^{\beta_n}}{r_0r_1^{\beta_n}}g_{-\beta,n}G^{(1)}_{\theta r} & 0 & 0 & 0 & 0\\
-\frac{f_{\alpha,n}G^{(1)}_{\theta r}}{r_0} & -\frac{f_{\beta,n}G^{(1)}_{\theta r}}{r_0} & -\frac{r_0^{\alpha_n}}{r_0r_1^{\alpha_n}}f_{-\alpha,n}G^{(1)}_{\theta r} & -\frac{r_0^{\beta_n}}{r_0r_1^{\beta_n}}f_{-\beta,n}G^{(1)}_{\theta r} & 0 & 0 & 0 & 0\\
\frac{r_0^{\alpha_n}}{r_1^{\alpha_n}}\phi_{\alpha,n} & \frac{r_0^{\beta_n}}{r_1^{\beta_n}}\phi_{\beta,n} & \phi_{-\alpha,n} & \phi_{-\beta,n} & -\frac{\left((n-1)+\kappa\right)\left(1+\nu^{(2)}\right)}{E^{(2)}r_1^{\,n-1}} & \frac{1+\nu^{(2)}}{E^{(2)}r_1^{\,n+1}} & -\frac{\left(\kappa-(n+1)\right)\left(1+\nu^{(2)}\right)r_1^{\,n+1}}{E^{(2)}} & \frac{\left(1+\nu^{(2)}\right)r_1^{\,n-1}}{E^{(2)}}\\
\frac{r_0^{\alpha_n}}{r_1^{\alpha_n}} & \frac{r_0^{\beta_n}}{r_1^{\beta_n}} & 1 & 1 & \frac{\left(\kappa-(n-1)\right)\left(1+\nu^{(2)}\right)}{E^{(2)}r_1^{\,n-1}} & \frac{1+\nu^{(2)}}{E^{(2)}r_1^{\,n+1}} & -\frac{\left(\kappa+(n+1)\right)\left(1+\nu^{(2)}\right)r_1^{\,n+1}}{E^{(2)}} & -\frac{\left(1+\nu^{(2)}\right)r_1^{\,n-1}}{E^{(2)}}\\
0 & 0 & 0 & 0 & \frac{(n-1)\left((n-1)+\kappa+\left(\kappa+(n+1)\right)\nu^{(2)}\right)}{\left(\nu^{(2)}-1\right)r_2^{\,n}} & \frac{(n+1)}{r_2^{\,n+2}} & -\frac{(n+1)\left(\kappa+\left((n-1)+\kappa\right)\nu^{(2)}-(n+1)\right)r_2^{\,n}}{\left(\nu^{(2)}-1\right)} & -(n-1)r_2^{\,n-2}\\
0 & 0 & 0 & 0 & -\frac{\left(n^2-n\right)}{r_2^{\,n}} & \frac{(n+1)}{r_2^{\,n+2}} & \left(n^2-n\right)r_2^{\,n} & (n-1)r_2^{\,n-2}
\end{bmatrix} \tag{B.5}$$

$$\hat{\mathbf{H}}^{*}_{n,2}=\begin{bmatrix}
\frac{r_0^{\alpha_n}}{r_1^{1+\alpha_n}}g_{\alpha,n}G^{(1)}_{\theta r} & \frac{r_0^{\beta_n}}{r_1^{1+\beta_n}}g_{\beta,n}G^{(1)}_{\theta r} & \frac{g_{-\alpha,n}G^{(1)}_{\theta r}}{r_1} & \frac{g_{-\beta,n}G^{(1)}_{\theta r}}{r_1} & \frac{(1-n)\left((n-1)+\kappa+\left(\kappa-(n+1)\right)\nu^{(2)}\right)}{\left(\nu^{(2)}-1\right)r_1^{n}} & -\frac{(n+1)}{r_1^{n+2}} & -\frac{(n+1)\left(\kappa+\left((n-1)+\kappa\right)\nu^{(2)}-(n+1)\right)r_1^{n}}{\left(\nu^{(2)}-1\right)} & (1-n)r_1^{n-2}\\
-\frac{r_0^{\alpha_n}}{r_1^{1+\alpha_n}}f_{\alpha,n}G^{(1)}_{\theta r} & -\frac{r_0^{\beta_n}}{r_1^{1+\beta_n}}f_{\beta,n}G^{(1)}_{\theta r} & -\frac{f_{-\alpha,n}G^{(1)}_{\theta r}}{r_1} & -\frac{f_{-\beta,n}G^{(1)}_{\theta r}}{r_1} & \frac{\left(n-n^2\right)}{r_1^{n}} & \frac{(n+1)}{r_1^{n+2}} & \left((n+1)^2-n-1\right)r_1^{n} & (1-n)r_1^{n-2}\\
\frac{g_{\alpha,n}G^{(1)}_{\theta r}}{r_0} & \frac{g_{\beta,n}G^{(1)}_{\theta r}}{r_0} & \frac{r_0^{\alpha_n}}{r_0r_1^{\alpha_n}}g_{-\alpha,n}G^{(1)}_{\theta r} & \frac{r_0^{\beta_n}}{r_0r_1^{\beta_n}}g_{-\beta,n}G^{(1)}_{\theta r} & 0 & 0 & 0 & 0\\
-\frac{f_{\alpha,n}G^{(1)}_{\theta r}}{r_0} & -\frac{f_{\beta,n}G^{(1)}_{\theta r}}{r_0} & -\frac{r_0^{\alpha_n}}{r_0r_1^{\alpha_n}}f_{-\alpha,n}G^{(1)}_{\theta r} & -\frac{r_0^{\beta_n}}{r_0r_1^{\beta_n}}f_{-\beta,n}G^{(1)}_{\theta r} & 0 & 0 & 0 & 0\\
\frac{r_0^{\alpha_n}}{r_1^{\alpha_n}}\phi_{\alpha,n} & \frac{r_0^{\beta_n}}{r_1^{\beta_n}}\phi_{\beta,n} & \phi_{-\alpha,n} & \phi_{-\beta,n} & -\frac{\left((n-1)+\kappa\right)\left(1+\nu^{(2)}\right)}{E^{(2)}r_1^{n-1}} & \frac{1+\nu^{(2)}}{E^{(2)}r_1^{n+1}} & \frac{\left(\kappa-(n+1)\right)\left(1+\nu^{(2)}\right)r_1^{n+1}}{E^{(2)}} & -\frac{\left(1+\nu^{(2)}\right)r_1^{n-1}}{E^{(2)}}\\
\frac{r_0^{\alpha_n}}{r_1^{\alpha_n}} & \frac{r_0^{\beta_n}}{r_1^{\beta_n}} & 1 & 1 & -\frac{\left(\kappa-(n-1)\right)\left(1+\nu^{(2)}\right)}{E^{(2)}r_1^{n-1}} & -\frac{1+\nu^{(2)}}{E^{(2)}r_1^{n+1}} & -\frac{\left(\kappa+(n+1)\right)\left(1+\nu^{(2)}\right)r_1^{n+1}}{E^{(2)}} & -\frac{\left(1+\nu^{(2)}\right)r_1^{n-1}}{E^{(2)}}\\
0 & 0 & 0 & 0 & \frac{(n-1)\left((n-1)+\kappa+\left(\kappa-(n+1)\right)\nu^{(2)}\right)}{\left(\nu^{(2)}-1\right)r_2^{n}} & \frac{(n+1)}{r_2^{n+2}} & \frac{(n+1)\left(\kappa+\left((n-1)+\kappa\right)\nu^{(2)}-(n+1)\right)r_2^{n}}{\left(\nu^{(2)}-1\right)} & (n-1)r_2^{n-2}\\
0 & 0 & 0 & 0 & \frac{\left(n^2-n\right)}{r_2^{n}} & -\frac{(n+1)}{r_2^{n+2}} & \left((n+1)^2-n-1\right)r_2^{n} & (n-1)r_2^{n-2}
\end{bmatrix} \tag{B.6}$$

For $2 \le n \le P$

$$\bar{k}=\{\bar{k}_0,\bar{k}_1,\cdots,\bar{k}_N\} \tag{B.7}$$

$$\bar{k}_0^{*}=\{0,0,-S_0,-\Sigma_0,0,0,0\} \tag{B.8}$$

$$\bar{k}_1^{*}=\begin{Bmatrix}0\\0\\0\\0\\0\\0\\0\\0\\0\\0\\0\\0\\0\end{Bmatrix};\bar{k}_1^{*}=\begin{Bmatrix}0\\0\\-S_{n,1}\\-\mathrm{T}_{n,2}\\0\\0\\-\Omega_{n,1}\\-\Psi_{n,2}\\0\\0\\-S_{n,2}\\-\mathrm{T}_{n,1}\\0\\0\\-\Omega_{n,2}\\-\Psi_{n,1}\end{Bmatrix} \tag{B.9}$$

References

[1] E.G. Kirsch, Die Theorie der Elastizität und die Bedürfnisse der Festigkeitslehre, Z. Verein. Deut. Ingen. 42 (1898).
[2] N.I. Muskhelishvili, Some Basic Problems of the Mathematical Theory of Elasticity, Noordhoff International Publishing, Leyden, 1977.
[3] S.G. Lekhnitskii, Theory of Elasticity of an Anisotropic Elastic Body, AIP Publishing, 1964.
[4] G. Savin, Stress Concentration Around Holes, Pergamon Press, 1961.
[5] M. Batista, On the stress concentration around a hole in an infinite plate subject to a uniform load at infinity, Int. J. Mech. Sci. 53 (2011) 254–261, https://doi.org/10.1016/J.IJMECSCI.2011.01.006.
[6] Y. Huang, R.K.N.D. Rajapakse, Practical stress solutions for single-edge V-notched tension specimen, Theor. Appl. Fract. Mech. 102 (2019) 193–209, https://doi.org/10.1016/J.TAFMEC.2019.04.011.
[7] M. Zappalorto, M. Ricotta, Understanding the effect of notches in orthotropic solids subjected to static loads, Theor. Appl. Fract. Mech. 116 (2021), 103110, https://doi.org/10.1016/J.TAFMEC.2021.103110.
[8] M. Zappalorto, P. Lazzarin, Stress fields due to inclined notches and shoulder fillets in shafts under torsion, J. Strain Anal. Eng. Des. 46 (2011) 187–199, https://doi.org/10.1177/0309324710396019.
[9] M. Zappalorto, P.A. Carraro, Stress distributions for blunt cracks and radiused slits in anisotropic plates under in-plane loadings, Int. J. Solids Struct. 56–57 (2015) 136–141, https://doi.org/10.1016/J.IJSOLSTR.2014.11.024.
[10] M. Pastrello, A. Pontefisso, M. Zappalorto, A new explicit solution for the mode I stress fields in notched orthotropic solids, Eur. J. Mech. A. Solids 97 (2023), 104819, https://doi.org/10.1016/J.EUROMECHSOL.2022.104819.
[11] M. Pastrello, M. Salviato, M. Zappalorto, Stress distributions in orthotropic solids with blunt notches under in-plane shear loadings, Eur. J. Mech. A. Solids 92 (2022), 104436, https://doi.org/10.1016/J.EUROMECHSOL.2021.104436.
[12] M. Zappalorto, P.A. Carraro, Two-dimensional stress distributions in tensioned orthotropic plates weakened by blunt V-shaped notches, Fatigue Fract. Eng. Mater. Struct. 40 (2017) 804–819, https://doi.org/10.1111/ffe.12554.
[13] D.S. Sharma, Stress distribution around polygonal holes, Int. J. Mech. Sci. 65 (2012) 115–124, https://doi.org/10.1016/J.IJMECSCI.2012.09.009.
[14] J. Rezaeepazhand, M. Jafari, Stress analysis of composite plates with a quasi-square cutout subjected to uniaxial tension, J. Reinf. Plast. Compos. 29 (2010) 2015–2026, https://doi.org/10.1177/0731684409341758.
[15] L. Quagliato, M. Ricotta, M. Zappalorto, S.C. Ryu, N. Kim, Notch effect in 20% short carbon fibre-PA reinforced composites under quasi-static tensile loads, Theor. Appl. Fract. Mech. 122 (2022), 103649, https://doi.org/10.1016/J.TAFMEC.2022.103649.
[16] M. Kazeruni, A. Ince, Data-driven artificial neural network for elastic plastic stress and strain computation for notched bodies, Theor. Appl. Fract. Mech. 125 (2023), 103917, https://doi.org/10.1016/J.TAFMEC.2023.103917.
[17] S. Karen Alavi, M.R. Ayatollahi, J. Jamali, M. Petru, On the applicability of digital image correlation method in extracting the higher order terms in stress field around blunt notches, Theor. Appl. Fract. Mech. 121 (2022), 103436, https://doi.org/10.1016/J.TAFMEC.2022.103436.
[18] A.A. Alshaya, A developed hybrid experimental–analytical method for thermal stress analysis of a deep U-notched plate, Theor. Appl. Fract. Mech. 124 (2023), 103753, https://doi.org/10.1016/J.TAFMEC.2023.103753.
[19] S. Cicero, S. Arrieta, M. Sánchez, L. Castanon-Jano, Analysis of additively manufactured notched PLA plates using failure assessment diagrams, Theor. Appl. Fract. Mech. 125 (2023), 103926, https://doi.org/10.1016/J.TAFMEC.2023.103926.
[20] A.R. Torabi, H. Talebi, M.R. Ayatollahi, M. Petru, Mixed mode I-III fracture resistance of stainless steel 316L weakened by V-notches with end holes, Theor. Appl. Fract. Mech. 122 (2022), 103574, https://doi.org/10.1016/J.TAFMEC.2022.103574.

[21] A.R. Torabi, B. Bahrami, M.A. Motamedi, H. Hasanvand, On the use of Brazilian disk specimen for measuring mixed-mode I/II translaminar fracture toughness of notched glass/epoxy composite laminates: a comprehensive study, Theor. Appl. Fract. Mech. 121 (2022), 103541, https://doi.org/10.1016/J.TAFMEC.2022.103541.
[22] R.C.J. Howland, On the stresses in the neighbourhood of a circular hole in a strip under tension, Philos. Trans. Roy. Soc. Lond. Ser. a, Contain. Papers Math. Phys. Charact. 229 (1930) 49–86, https://doi.org/10.1098/rsta.1930.0002.
[23] C.-B. Ling, Stresses in a Notched Strip Under Tension, J. Appl. Mech. 14 (1947) A275–A280, https://doi.org/10.1115/1.4009733.
[24] T. Wah, Stresses in polygonal plates with circular holes, Eng. Fract. Mech. 23 (1986) 489–493, https://doi.org/10.1016/0013-7944(86)90157-8.
[25] Z. Pan, Y. Cheng, J. Liu, Stress analysis of a finite plate with a rectangular hole subjected to uniaxial tension using modified stress functions, Int. J. Mech. Sci. 75 (2013) 265–277, https://doi.org/10.1016/J.IJMECSCI.2013.06.014.
[26] C.-C. Lin, C.-C. Ko, Stress and strength analysis of finite composite laminates with elliptical holes, J. Compos. Mater. 22 (1988) 373–385, https://doi.org/10.1177/002199838802200405.
[27] X. Xu, L. Sun, X. Fan, Stress concentration of finite composite laminates with elliptical hole, Comput. Struct. 57 (1995) 29–34, https://doi.org/10.1016/0045-7949(94)00588-T.
[28] M. Salviato, M. Zappalorto, A unified solution approach for a large variety of antiplane shear and torsion notch problems: theory and examples, Int. J. Solids Struct. 102–103 (2016) 10–20, https://doi.org/10.1016/J.IJSOLSTR.2016.10.022.
[29] M. Salviato, M. Zappalorto, L. Maragoni, Exact solution for the mode III stress fields ahead of cracks initiated at sharp notch tips, Eur. J. Mech. A. Solids 72 (2018) 88–96, https://doi.org/10.1016/J.EUROMECHSOL.2018.04.014.
[30] M. Pastrello, A. Pontefisso, M. Zappalorto, Exact in-plane stress field solution for isotropic plates with circular holes reinforced with cylindrically orthotropic rings, Theor. Appl. Fract. Mech. 125 (2023), 103821, https://doi.org/10.1016/J.TAFMEC.2023.103821.
[31] J.M. Dave, D.S. Sharma, Stress field around rectangular hole in functionally graded plate, Int. J. Mech. Sci. 136 (2018) 360–370, https://doi.org/10.1016/J.IJMECSCI.2017.12.010.
[32] Q. Yang, C. Gao, W. Chen, Stress concentration in a finite functionally graded material plate, Sci. China Phys. Mech. Astron. 55 (2012) 1263–1271, https://doi.org/10.1007/s11433-012-4774-x.